Aerodynamic Characteristics of Spinning Bodies of Revolution

by

SAMIRA ABDEL-KAWY

of the
Department of Aeronautics and Astronautics
University of Southampton

A Thesis submitted for the Degree of
Master of Philosophy

1975

Contents

ABSTRACT

The complete knowledge of the aerodynamic forces during the flight of shells and missiles is essential to the study of the flight mechanics of these objects. One of the most complicated type of aerodynamic force to predict, in a general case, is that produced whenever the spinning axis is at an angle of incidence to the free stream velocity vector. This phenomenon is commonly known as the Magnus effect. The only theories developed to date assume small angles of incidence and are based on a laminar boundary layer development around the body which has not separated. This study is an attempt to produce more information concerning quantitative estimates of the Magnus effect.

ACKNOWLEDGEMENTS

I should like to offer my thanks to many people who have assisted me during the preparation of this thesis. They include Dr. M. Judd, Dr. M.J. Goodyer and Professor G.M. Lilley who made this research possible. The guidance and encouragement they gave during the preparation of this work are gratefully acknowledged. The members of the Aeronautics Department, workshop staff and the computer staff are thanked for their cooperation.

Last, but not least, my deep gratitudes are due to my parents for their patience and understanding.

Notation

A	Constant
A,B,C	Matrices
a_i, b_i, c_i	Constant
a	Body radius, sonic speed
D	Drag
D,E	Integrals
d	Body diameter
d_1, d_2, d_3	Constants

Corrigenda

Page Number	Line Number			
		Alteration		
11	5	"ωa/v"	to be	"ωa/U".
29	7	"U"	to be	"Usinα"
29	16	"$\left(\frac{\ell}{a}\right)^3$"	to be	"$\left(\frac{\ell}{a}\right)^2$"

U	Free stream velocity
x,y,z	Cartesian coordinate system
u,v,w	Velocity component in x, y and z direction
$\bar{u}, \bar{v}, \bar{w}$	Nondimensional velocity components u/U, v/U and w/U
$F_{m1}, F_{m2}, F_{m3}, F_{m4}$	Magnus force component
F	Aerodynamic force, complex potential
I_a, I_f, I_d	Aft, fore and drag current
c_L, c_D, c_Z	Lift, drag, normal force coefficient

c_M	Pitching moment coefficient referring to the nose
$M_{m1}, M_{m2}, M_{m3}, M_{m4}$	Magnus moment component referring to body nose
$K_{f1}, K_{f2}, K_{f3}, \ldots$	Magnus force coefficient $F_{m1}/q_\infty S, \ldots$
$K_{m1}, K_{m2}, \ldots$	" moment " $M_{m1}/q_\infty Sd$
c_p	pressure coefficient
Z, Z_1, Z_2	Complex coordinate
$\bar{x}_p$	Centre of pressure
F	Complex potential
$\bar{w}$	potential velocity in z direction
F_t, M_t	Total Magnus force and moment
K_{ft}, K_f	Magnus force coefficient $F_t/q_\infty S$
K_{mt}, K_m	" moment " $M_t/q_\infty Sd$
r, φ, x	Cylindrical polar coordinate
v_r, v_φ, v_x	velocity component in r, φ and x direction
$h(x,z)$	boundary layer edge
u_p, w_p	velocity component at the edge of the boundary layer
s_1, s_2	position of boundary layer separation
α	angle of incidence
ω	angular velocity
$\bar{\omega}$	spin rate $\omega a/U$
ρ	density
δ, δ_x, δ_z	boundary layer thickness in x and z directions
Δ	boundary layer displacement thickness
ν	kinematic viscosity
η	Blasius similarity parameter $\frac{y}{x}\sqrt{\frac{Ux}{\nu}}$
ψ	Stream function
ψ_1, ψ_2	separation position angle
θ	angle
θ_o	forward stagnation point angle

$\Gamma, \Gamma_1, \Gamma_2$	Vortex strength
τ	Skin friction
i	$\sqrt{-1}$
$( )'$	first derivative
$( )''$	second "
$( )_o$	zero order in α or $\bar{\omega}$
$( )_1$	first order in α or $\bar{\omega}$
$( )_2$	second " in α or $\bar{\omega}$
$\frac{\partial}{\partial}$	partial derivative
∇^2	$\frac{\partial^2}{\partial x^2} + \frac{\partial^2}{\partial y^2} + \frac{\partial^2}{\partial z^2}$
grad	$\frac{\partial}{\partial x}\underline{i} + \frac{\partial}{\partial y}\underline{j} + \frac{\partial}{\partial z}\underline{k}$

List of Figures

CHAPTER I

Introduction and Historical Background

I.1 Introduction:

A side force is developed on rotating bodies of revolution such as spinning shells and missiles whenever the axis of spin is at an angle to the direction of motion. This force and its moment are the result of what is known as the "Magnus effect". This effect is aerodynamic in origin and is the direct result of the flow of air over the body. The interaction between rotation and the cross flow velocity produces an asymmetric flow field. The Magnus force acts perpendicular to the plane containing the spin axis and the free stream velocity vector. The convention for the force, spin direction and incidence is shown in fig (I.1). The asymmetry in the boundary layer thickness distribution alters the effective aerodynamic shape of the body and this is one of the factors giving rise to the production of the side force and moment.

Measurements* [1] show that the variation of the nondimensional Magnus force and moment coefficients with spin rate and incidence are of similar form, for each body length to diameter ratio (ℓ/d). The local Magnus force loading coefficient is a function of the axial position but is independent of the overall length of the body. At angles of incidence up to 10° the variation of the side force and moment coefficient with spin rate is approximately linear in agreement with theory [2] . The Magnus force is in the positive direction and is of order between 5 to 40% of the lift force for Reynolds numbers (based on body diameter) of the order $2 \cdot 10^5$. The theoretical slender body lift is, however,

---

* Bibliography mentioned after the References.

unaffected by the spin even allowing for the viscous effects. The effects of the body spin on the normal force and pitching moment are small enough to be neglected for an angle of incidence up to about 10°. At larger incidences the effect of spin becomes noticeable and is a function of the body length to diameter ratio (ℓ/d).

The Magnus force and moment can be important in the prediction of projectile behaviour in flight. The aerodynamic stability and flight trajectories of spinning shells and missiles are both sensitive to the magnitude and direction of the Magnus force and moment.

The prediction of the Magnus force and moment is very complicated. Early attempts to develop a satisfactory theory[2] assumed small values of non-dimensional spin rate $\omega a/U$ (see Notation) and small angle of incidence α such that $\alpha\ell/d << 1.0$. This theory assumed a laminar unseparated boundary layer. The corresponding predicted Magnus force varies linearly with $\omega a/U$, α and is inversely proportional to the square root of Reynolds number ($U\ell/\nu$) and acts in the positive direction, in agreement with experiments[3]. It was found that the Magnus force and its moment could be correlated with the distortion of the boundary layer displacement thickness distribution resulting from the body spin.

At angles of incidence greater than 10° measurements[3] show that the Magnus force and moment variations with spin parameter $\bar{\omega}$ become highly non-linear. At this incidence the flow in each cross flow plane is analogous to that of the flow over a two dimensional circular cylinder impulsively started from rest whilst rotating. The effect of the incidence on vortex formation as the spin is increased have been visualized using smoke[4]. For angles of incidence between zero and 4°, it was noticed that the vortices which develop on the leeward side merge with

the boundary layer and may be regarded as an integrated part of it; a definite hump was present on the advancing side of the body and there is a minimum boundary layer thickness on the retreating side. This boundary layer local thickness rotates around the body as it spins up. This agrees well with the computation of the boundary layer displacement thickness and a complete analysis is presented in chapter II. As the angle of incidence increases, the boundary layer separates as two vortex sheets which roll up into two vortices on the lee side of the cylinder as illustrated in fig. (I.2) for the rotating and non-rotating cases. The presence of the vortices modifies the pressure distribution around the cylinder in the cross flow plane and consequently the boundary layer characteristics. It is this aspect of the flow phenomenon which is considered in this thesis. A comparison is made between the different contributions to the Magnus force and moment which result from the boundary layer displacement thickness distortion, in order to predict which dominates at small angles of incidence. At large angles of incidence it is the generation of the asymmetric vortex pair that controls the Magnus force and moment. The vortex flow features will be discussed in detail in chapter III.

I.2 Historical Background:

In 1671 Walker[5] described the deviation of the sliced tennis ball and he was followed by Rabin in 1736 who explained the dispersion of a spinning canon ball. The first crude experiment was carried out by G. Magnus in 1852, after whom the phenomenon of the production of a side force resulting from spinning was named. G. Magnus related the drift of a spinning projectile to the aerodynamic force produced by the interaction between the body rotation and the flight velocity, through the

asymmetric pressure distribution. In a paper published by Lord Rayleigh [6] in 1877 on "The irregular flight of a tennis ball" the ideal flow representation of the classical potential flow field around a circular cylinder with circulation was used as a mathematical model for the development of the required circulation. However, the relationship between Magnus force and spin rate could not be determined from this theory. In the case of a uniform flow of a real fluid past a spinning two dimensional circular cylinder a lift is developed which is the Magnus force in the case of three dimensional flow.

Qualitative data and negative Magnus force at low rotational speed were first obtained by Lafay in the period between 1910 and 1912. The first practical application in producing lift was the Flettner rotor developed in Gottingen. The long range flight of dimpled golf ball was also explained qualitatively in terms of the generation of a turbulent boundary layer, delayed separation and a consequent reduction in drag. An attempt to employ the spinning cylinder as a part of a high lift wing was unsuccessful in the early days of aviation although it has been incorporated in recent times with more success in an experimental NASA aircraft.

In recent work Martin [2] considered a flow in which no wake is formed on the leeward side of the body. A laminar boundary layer analysis, on a cylindrical portion of a slender body of revolution having a small angle of incidence and small spin rate, showed that the boundary layer displacement thickness distortion could cause a Magnus force of the proper direction. In 1954 Kelly [7] discussed Martin's theory and proposed an improved coordinate system to permit a more exact solution. He also criticised the numerical values obtained by Martin and their lack of numerical accuracy. Kelly and Thacker [8] extended the theory

to include additional terms in higher order spin rate. Platou[6] suggested an empirical method based on the lift force, of a circular cylinder in a cross flow, as a treatment for the case of high angle of incidence. Power[10] followed Kelly's procedure and included the effect of the axial circulation distribution.

Magnus force and moment measurements have been carried out by many people and recently a number of extensive tests[1] and[3] have been made in Australia using a model with ogive nose on a cylindrical body. These tests covered a wide range of incidence and spin for different Reynolds numbers and body length to diameter ratios (ℓ/d). Measurements of the boundary layer separation positions showed that it is dependent on the spin rate and independent of the vortex core locations over a given range of Reynolds number. The negative Magnus force was explained using an impulsive flow analogy at a critical Reynolds number range between 10^5 to $5 \cdot 10^5$, based on body diameter. This negative Magnus force was shown to be dependent on the asymmetric growth of the boundary layer around the body cross section in the cross flow plane.

The role of the boundary layer in producing Magnus force is dominant only when the flow around the body is fully attached. When the boundary layer separates, the rwo feeding vortex sheets are convected downstream to form the wake and these control the production of Magnus force. The boundary layer development is then of less importance in the generation of Magnus force.

The purpose of the work presented here is to extend the existing theory of Martin and Kelly to allow for higher angles of incidence and higher spin rates. The work concentrates on the

presence of the potential flow vortices on the leeward side of the cylinder and how they affect the boundary layer characteristics and consequently the Magnus force. The model for the flow separation is a simplified extension of those methods used in the prediction of the effect of leading edge separation on slender wing plan forms[19,20] in the case of the wing, the separation points in the cross flow plane are well-defined and, on transforming the potential flow to that about a cylinder, such points become stagnation points of the cross flow plane. the strengths of the standing vortices are such as to maintain the locations of these points. In applying these ideas to the body of revolution at least three major differences can arise:-

1. Stand-off distances are not so great and at low angles of attack the vortices merge with the boundary layer and are weak.

2. With increasing incidence the vortices form sets reminiscent of the vortex street of the two-dimensional cylinder flow. However, the leading vortex is by far the strongest of the set and a reasonable simplification is achieved by assuming a single vortex on each side.

3. The locations of the separation points are no longer well-defined but require a full understanding of the three-dimensional boundary layer separation behaviour on spinning bodies of revolution.

To overcome these difficulties a semi-empirical model was developed having the following features:-

a. A single pair of potential flow vortices of unknown strength and location.

b. The stand-off distances are large compared with the boundary layer thickness.

c. At the edge of the boundary layer and at the separation lines the total circumferential velocity component of the external potential flow is zero and the axial velocity components are discontinuous giving rise to the feeding vortex sheets.

The vortex strengths can again be determined by ensuring stagnation points in the cross flow plane coincident with the actual separation points at that axial station.* This is consistent with observed streamline patterns on non-spinning bodies at moderate to large angles of attack. To avoid the complexities and innaccuracies inherent in the prediction of the separation points, the measured locations derived from wind tunnel tests are used to give an empirical variation with incidence, spin ratio and Reynolds number. One limitation of this approach is the limited amount of data available.

In the slender wing theories [19,20] which take accounts of leading edge separation, it is found necessary to include the effect of the feeding sheet in the cross-flow boundary conditions. In the present application, body shapes tend to be much more slender with large portions of the length having constant cross section area. The feeding sheets will therefore be much weaker and the axial variation of the vortex strengths will be slower. It is therefore assumed that the cross-flow is dominated by the standing vortices, that the detailed feeding sheet geometry need not be considered and that the force-free boundary condition need be applied to the concentrated vortices alone.

* The assumption that the separation and cross-flow stagnation points coincide is not the only possibility. Other criteria for the location of the separation points may prove to be more valid.

The contributions of the present work fall into two distinct sections. In Chapter II and Appendix A, the analysis of the asymmetric boundary layer growth for low incidence attached flow is extended to include higher order terms in the incidence and spin ratio. In Chapter III and Appendix B, the high incidence case is analysed using the vortex model introduced above. From these results the various Magnus force components have been calculated. The constituent parts of the Magnus force that have been included are as follows:-

1. Normal pressure distribution arising from:
    a. asymmetric boundary layer growth.
    b. asymmetric potential flow outside the boundary layer.
    c. the centrifugal field in the boundary layer.
2. Skin friction components.

The relative magnitudes of these contributions over the incidence range are considered in Chapter IV and the theoretical results are compared with measured values.

CHAPTER II

Boundary Layer Characteristics of a Rotating Body of Revolution

II.1 Equations of Motion:

The steady viscous incompressible flow about a rotating cylinder of length ℓ and constant diameter d is considered for the case when it is placed at a small incidence α to a uniform stream. The uniform flow has a speed U, the cylinder rotates with an angular velocity ω, which is taken as positive in the clockwise direction when facing the nose of the cylinder. The spin parameter is defined as $\bar{\omega} = \omega a/U$.

The nose portion of the cylinder is assumed to have a negligible effect on the boundary layer development beyond a certain distance downstream of the nose. Thus, the detailed boundary layer growth on the nose and any separation and reattachment downstream of the nose are not considered in this analysis. A rough method to include these effects is based on the assumption that the length of the main cylindrical body [2] is effectively increased by an amount equal to the half length of the nose. The flow at a small angle of attack is assumed to be attached over the entire length of the body, and for this case the Reynolds number is assumed to be in a range such that laminar boundary layer flow exists everywhere.

A set of non-rotating axes, fixed in the body, is used in this analysis and is illustrated in fig. (II.1). The Navier Stokes equations of motion and the continuity equation are first written in cylindrical polar coordinates, with the x-axis coincident with the cylinder axis. The corresponding Prandtl boundary layer equations are developed with the appropriate boundary conditions at the body surface and in the free

stream outside the boundary layer. The inviscid flow outside the boundary layer is obtained from slender body theory. The Navier-Stokes equations for the radial, circumferential and axial directions are respectively:

$$\left.\begin{aligned}
&v_r \frac{\partial v_r}{\partial r} + \frac{v_\varphi}{r}\frac{\partial v_r}{\partial \varphi} + v_x \frac{\partial v_x}{\partial x} - \frac{v_\varphi^2}{r} = -\frac{1}{\rho}\frac{\partial P}{\partial r} + \\
&\nu\left[\frac{\partial^2 v_r}{\partial r^2} + \frac{1}{r}\frac{\partial v_r}{\partial r} - \frac{v_r}{r^2} + \frac{1}{r^2}\frac{\partial^2 v_r}{\partial \varphi^2} + \frac{\partial^2 v_r}{\partial x^2} - \frac{2}{r^2}\frac{\partial v_\varphi}{\partial \varphi}\right] \\
&v_r \frac{\partial v_\varphi}{\partial r} + \frac{v_\varphi}{r}\frac{\partial v_\varphi}{\partial \varphi} + \frac{v_r v_\varphi}{r} + v_x \frac{\partial v_\varphi}{\partial x} = -\frac{1}{\rho r}\frac{\partial P}{\partial \varphi} + \nu\left(\frac{\partial^2 v_\varphi}{\partial r^2} + \frac{1}{r}\frac{\partial v_\varphi}{\partial r} - \right. \\
&\left.\frac{v_\varphi}{r^2} + \frac{1}{r^2}\frac{\partial^2 v_\varphi}{\partial \varphi^2} + \frac{2}{r^2}\frac{\partial v_r}{\partial \varphi} + \frac{\partial^2 v_\varphi}{\partial x^2}\right) \\
&v_r \frac{\partial v_x}{\partial r} + \frac{v_\varphi}{r}\frac{\partial v_x}{\partial \varphi} + v_x \frac{\partial v_x}{\partial x} = -\frac{1}{\rho}\frac{\partial P}{\partial x} + \nu\left(\frac{\partial^2 v_x}{\partial x^2} + \frac{1}{r}\frac{\partial v_x}{\partial r} + \frac{1}{r^2}\frac{\partial^2 v_x}{\partial \varphi^2} + \frac{\partial^2 v_x}{\partial r^2}\right)
\end{aligned}\right\} \qquad \text{(II.1)}$$

The continuity equation is

$$\frac{\partial v_r}{\partial r} + \frac{v_r}{r} + \frac{1}{r}\frac{\partial v_\varphi}{\partial \varphi} + \frac{\partial v_x}{\partial x} = 0 \qquad \text{(II.2)}$$

where v_r, v_φ and v_x are the velocity components in r, φ and x directions.

The Prandtl boundary layer assumptions are used i.e. the boundary layer thickness δ is small compared with both the body length ℓ and the body radius a. Hence the following orders of magnitude may be written:

$$\frac{v_x}{U} = O(1)$$

$$\frac{v_r}{U} = O\left(\frac{\delta}{\ell}\right)$$

$$\frac{v_\phi}{U} = O\left(\frac{\omega a}{U}\right)$$

$$\frac{\partial}{\partial x} = O(\ell^{-1})$$

$$\frac{\partial}{\partial r} = O(\delta^{-1})$$

$$\frac{1}{r}\frac{\partial}{\partial \phi} = O(a^{-1})$$

It is assumed that the spin ratio $\omega a/v$ is O(1) and terms of this order are retained. Terms involving $\omega \ell/U$ will be $O(\ell/a)$ but it is not assumed that these will dominate since ℓ/a may have modest values for some body shapes of practical interest.

Equations (II.1) and (II.2) reduce to:-

$$v_r \frac{\partial v_\phi}{\partial r} + \frac{v_\phi}{a}\frac{\partial v_\phi}{\partial \phi} + v_x \frac{\partial v_\phi}{\partial x} = -\frac{1}{\rho a}\frac{\partial p}{\partial \phi} + \nu \frac{\partial^2 v_\phi}{\partial r^2}$$

$$v_r \frac{\partial v_x}{\partial r} + \frac{v_\phi}{a}\frac{\partial v_x}{\partial \phi} + v_x \frac{\partial v_x}{\partial x} = -\frac{1}{\rho}\frac{\partial p}{\partial x} + \nu \frac{\partial^2 v_x}{\partial r^2} \qquad \text{(II.3)}$$

$$0 = \frac{\partial p}{\partial r}$$

and $$\frac{\partial v_r}{\partial r} + \frac{1}{a}\frac{\partial v_\phi}{\partial \phi} + \frac{\partial v_x}{\partial x} = 0$$

Because of the modest values of spin ratio ($\omega a/U$) permitted in these equations, the centrifugal term v_ϕ^2/r has a negligible contribution and, to this order the pressure is constant in the radial direction. However, the Magnus force depends on higher order asymmetries in the boundary layer distribution and the radial variation of pressure has a small but significant effect on the normal pressure at the surface. The corresponding effect on the Magnus force can be readily estimated once the solution for v_ϕ has been obtained. Equation set (11.3) applies to both axi-symmetric and non-axisymmetric flows and can be used for the case of a body set at incidence α to the free stream direction.

Provided the boundary layer thickness is everywhere very small compared with the local cross-section radius, the cylindrical coordinates r, and x can be replaced by a set of curvi-linear surface coordinates x, y and z such that:-

$$\frac{\partial}{\partial x} = \frac{\partial}{\partial x}$$

$$\frac{\partial}{\partial y} = \frac{\partial}{\partial r}$$

and $$\frac{\partial}{\partial z} = \frac{1}{a}\frac{\partial}{\partial \phi}$$

Then equations (II.3), are replaced by:

$$\left.\begin{aligned} u\frac{\partial u}{\partial x} + v\frac{\partial u}{\partial y} + w\frac{\partial u}{\partial z} &= -\frac{1}{\rho}\frac{\partial P}{\partial x} + \nu\frac{\partial^2 u}{\partial y^2} \\ u\frac{\partial w}{\partial x} + v\frac{\partial w}{\partial y} + w\frac{\partial w}{\partial z} &= -\frac{1}{\rho}\frac{\partial P}{\partial z} + \nu\frac{\partial^2 w}{\partial y^2} \\ \frac{1}{\rho}\frac{\partial P}{\partial y} &= 0 \\ \frac{\partial u}{\partial x} + \frac{\partial v}{\partial y} + \frac{\partial w}{\partial z} &= 0 \end{aligned}\right\} \qquad \text{(II.4)}$$

where u, v and w are the velocity components in the directions x, y and z shown in fig. (II.1). Equations (II.4) form the general three dimensional laminar boundary layer equations.

II.2 Boundary Conditions:

In solving the boundary layer equations (II.4) the boundary conditions on the cylinder surface and at the outer edge of the boundary layer have to be satisfied. The velocity components on the body surface are $u = v = 0$ and $w = \omega a$. The velocity components outside the boundary layer depend on the inviscid outer flow. Using slender body theory, it is found that

$$u = U\cos\alpha$$

$$w = 2U\sin\alpha\,\sin(z/a)$$

and the pressure gradients are given by

$$-\frac{1}{\rho}\frac{\partial P}{\partial z} = 4U^2(\sin\alpha)^2\sin(z/a)\cos(z/a)/a$$

and

$$\frac{\partial P}{\partial x} = 0$$

II.3 Solution of Boundary Layer Equations:

The solution of the boundary layer equations (II.4) may be developed to include higher order terms in the spin parameter $\bar{\omega}$ and incidence α. Using perturbation analysis, the velocity components are assumed to have the following form:

$$\left.\begin{aligned} \bar{u} &= \frac{u}{U} = u_o + u_1 + u_2 + u_3 + u_4 + \cdots \\ \bar{v} &= \frac{v}{U} = v_o + v_1 + v_2 + v_3 + v_4 + \cdots \\ \bar{w} &= \frac{w}{U} = w_1 + w_2 + w_3 + w_4 + \cdots \end{aligned}\right\} \qquad \text{(II.5)}$$

where u_o and v_o are the velocity components for zero incidence and zero spin, subscripts 1, 2 and 3 correspond to the order of perturbation quantities in α and/or $\bar{\omega}$. The details of the solution are given in appendix A. The expressions for the velocity components which satisfy the differential equations (II.4) and the boundary conditions are given by:

$$\begin{aligned} \bar{u} &= f_o'(\eta) + \alpha x/a\, f_1(\eta)\cos(z/a) + \alpha\,\bar{\omega}\,(\tfrac{x}{a})^2 f_2(\eta)\sin(z/a) \\ &\quad + \alpha\,\bar{\omega}^2\,(\tfrac{x}{a})^3 f_6(\eta)\cos(z/a) + \alpha\,\bar{\omega}^3\,(\tfrac{x}{a})^4 f_7(\eta)\sin(z/a) + \\ &\quad \alpha^2(\tfrac{x}{a})^2\,(f_3(\eta) + f_4(\eta)\cos(2a/a)) - \alpha^2/2\, f_5'(\eta) + \cdots \end{aligned}$$

$$\begin{aligned} \bar{v} &= \sqrt{\tfrac{\nu}{Ux}}\,\{\tfrac{1}{2}(\eta f_o'(\eta) - f_o(\eta) + \tfrac{\alpha x}{a}\, g_o(\eta)\cos(z/a) + \\ &\quad \alpha\,\bar{\omega}\,(\tfrac{x}{a})^2 g_1(\eta)\sin(z/a) + \alpha\,\bar{\omega}^2\,(\tfrac{x}{a})^3 g_4(\eta)\cos(z/a) + \\ &\quad \alpha\,\bar{\omega}^3\,(\tfrac{x}{a})^4 g_5(\eta)\sin(z/a) + \alpha^2(\tfrac{x}{a})^2(g_2 + g_3\cos(2z/a)) \\ &\quad - \alpha^2/4\,(\eta f_5'(\eta) - f_5(\eta))\} + \cdots \end{aligned}$$

$$\bar{w} = \bar{\omega}(1 - f_o'(\eta)) + 2\alpha f_o'(\eta) \sin(z/a) + \alpha \bar{\omega} \frac{x}{a} h_o(\eta) \cdot \cos(z/a) +$$

$$\alpha \bar{\omega}^2 \left(\frac{x}{a}\right)^2 h_1(\eta) \sin(z/a) + \alpha^2 \frac{x}{a} h_2(\eta) \sin(2z/a) +$$

$$\alpha \bar{\omega}^3 \left(\frac{x}{a}\right)^3 h_3(\eta) \cos(z/a) \qquad \text{(II.6)}$$

where

$$\eta = \frac{y}{x} \sqrt{\frac{Ux}{\nu}}$$

and f_n, g_n and h_n are perturbation functions which satisfy the ordinary differential equations developed in Appendix A. The numerical values of the perturbation functions are tabulated in Appendix A.

A set of the velocity profiles defined by equations (II.6) have been obtained using the ICL 1907 digital computer for given values of α, $\bar{\omega}$ and x/a. Details of computation are given in appendix A. Some examples of these velocity profiles are shown in fig. (II.2).

II.4 Boundary Layer Characteristics:

Moore [10] has derived an expression for the boundary layer displacement thickness Λ for a three dimensional flow over a non rotating surface. This expression is also valid for moving surfaces. It is given by the following partial differential equation, the derivation of which is described in Appendix C:-

$$\frac{\partial}{\partial x}(\Lambda - \delta_x) + \frac{\partial}{\partial z}(\Lambda - \delta_z) \frac{w_p}{U_p} = 0 \qquad \text{(II.7)}$$

where Λ is the boundary layer displacement thickness.

$$\left.\begin{aligned} \delta_x &= \int_0^{\delta} \left(1 - \frac{u}{U_p}\right) dy \\ \delta_z &= \int_0^{\delta} \left(1 - \frac{w}{w_p}\right) dy \\ w_p &= 2U \sin\alpha \sin(z/a) \\ \text{and } U_p &= U \cos\alpha \end{aligned}\right\} \qquad (II.8)$$

Substituting from equations (II.8) into (II.7) gives:-

$$\frac{\partial}{\partial x}\left(\Delta - \int_0^{\delta} \left(1 - \frac{u}{U_p}\right) dy\right) + \frac{\partial}{\partial z}\left(\Delta - \int_0^{\delta} \left(1 - \frac{w}{w_p}\right) dy\right) \frac{w_p}{U_p} = 0 \qquad (II.9)$$

Finally, by substituting equations (II.6) into (II.9) and integrating along the body axis, the displacement thickness is obtained in the form

$$\Delta = \sqrt{\frac{\nu x}{U}}\left\{ F_o - \frac{\alpha x}{a}\cos(z/a)\, F_1 - \alpha\bar{\omega}\left(\frac{x}{a}\right)^2 \left(F_2 - \frac{2}{5}H_o\right)\sin(z/a) - \right.$$

$$\alpha\bar{\omega}^2\left(\frac{x}{a}\right)^3\left(F_6 + \frac{2}{7}H_1\right)\cos(z/a) - \alpha\bar{\omega}^3\left(\frac{x}{a}\right)^4\left(F_7 - \frac{2}{9}H_3\right)\sin(z/a) +$$

$$\left.\frac{\alpha^2}{2}\left(F_5 - \eta - F_o\right) - \alpha^2\left(\frac{x}{a}\right)^2\left(F_3 + \left(F_3 + \frac{2}{5}H_2 - \frac{4}{5}F_1\right)\cos(2z/a)\right)\right\} + \ldots$$

(II.10)

where F_o, F_1, F_2, ... and

H_o, H_1, H_2, H_3 involve integrals of the perturbation functions and are defined in appendix A.

The details of the boundary layer displacement thickness calculations can be found in Appendix C. A typical boundary layer displacement thickness distribution for given values of α, $\bar{\omega}$ and x/a is presented in fig. (II. 4), for a particular value of Reynolds number $\left(\frac{u\ell}{\nu}\right)$.

CHAPTER III

Vortex Flow Analysis

III.1 Introduction

At angles of attack about 5^{o} the origin of Magnus force differs from that used in the analysis of Martin [2]. The assumption of an attached thin boundary layer development around the body no longer applies. A boundary layer separation exists with vortex sheets rolling up to form an asymmetric vortex pair located above the body. The flow around a slender body of revolution was described by Allen [11], Kelly [12] and others as being similar, in each cross flow plane, to the flow around a two dimensional circular cylinder. Buford [13] and Platou [6] have suggested that the Magnus force on a given cross section of the spinning body is related to that of a spinning circular cylinder with its axis normal to the free stream direction. However the relevant force, on each cross section, is not the steady force but is the force on a rotating cylinder impulsively started from rest.

The flow over an impulsively started circular cylinder leads to an axial circulation distribution dominated by the net circulation of the vortex pair. The analytical study of the early phases of the fluid motion around a body which is started impulsively from rest was first considered by Blasius. It was found that after a lapse of time the boundary layer separates from the cylinder surface. The time and location of the separation depends on the Reynolds number and the axial position. The separation points move rapidly around the cylinder until at large values of time they coincide with the points of laminar separation for steady flow. Kelly [12] and Bryson [14] have adapted the model illustrated in fig. (III.1)

for the development of the cross flow circulation with distance along an inclined body of uniform diameter for a symmetric shedding of circulation.

III.2 Development of Circulation:-

In viscous fluid flow the boundary layer is a region adjacent to the surface whose motion is governed by the fluid viscosity. This layer can be thought of as a thin sheet of vorticity being convected along and diffused away from the surface. This vorticity is shed into the outer flow at the position of the separation of the boundary layer from the body surface. Similarly the effect of the surface movement is transmitted through the boundary layer into the external potential flow. Fig. (III.1) shows the positions of the boundary layer separation and the formation of the separated vortex sheets which convect downstream and form the wake. The circulation strength at any instant is equal and opposite to the net vorticity that has been shed in a manner similar to the growth of circulation around an airfoil. The amount of circulation developed about the whole cylinder reflects on the pressure distribution over it, producing a lift force and, whenever the body is rotating, a side force is generated. The separated flow vortex sheets, being unstable, roll up into spiral vortices. Hence, after diffusion has taken place, the vorticity is concentrated largely in the vortex core. Vorticity is fed into the vortex core continuously through the feeding separated flow vortex sheets which connect to the attached boundary layer at the separation lines.

In the case of high fineness ratio bodies of revolution [15] a side force can be developed without spin due to the asymmetric pattern of vortices shed alternatively from either side of the cylinder. Near the body nose the boundary layer is thin and attached but further downstream two symmetric vortices are shed from the leeward side of the body. At a sufficient distance along the body these vortices detach and move down-

stream at an angle relative to the free stream. Further downstream other vortex sheets form and detach from both sides of the body. Hence at any cross flow plane, the wake has the appearance of, at least, part of a vortex street as illustrated in fig.(III.2). When spin is introduced, a similar pattern exists although the position of the separated vortex sheets and the corresponding rolled up vortices are different.

The development of separated vortex sheets is governed by two approximate conditions. First, there must be a force balance on the concentrated vortex and its feeding sheets i.e. zero net force on the system composed of the vortex and the feeding sheet.* This derives from the physical requirement that the fluid pressure should be continuous throughout the flow field. The second condition is that the separated vortex sheets start from the boundary layers at their points of separation. The condition for boundary layer separation depends on the pressure distribution outside the boundary layer near the separation. The pressure distribution itself depends on the positions and strength of the rolled up vortex sheets. This interdependence between the viscous boundary layer flow, its separation and the potential flow arising from the separated vortex sheets is complex and it is necessary to resort to a simple flow model. The model used here is shown in fig. (III.1) and is composed of two vortices located in the leeward side of the cylinder. Initially a potential flow is assumed and a solution is formed for the body and concentrated vortices satisfying the approximate boundary conditions at infinity and on the body surface. As part of the solution the position and strength of the concentrated vortices will be found for given separation points. In the case of the body of revolution, the position of the boundary layer separation is complex to predict being dependent on the flow Reynolds number and boundary conditions on the body surface. The

* As discussed in the Introduction, the feeding sheet strength will be small and for the present model its force contribution is neglegted.

positionsof the separation lines also depend on the condition of the boundary layer ahead of separation. For the above mentioned flow model, the position of separation is to be determined empirically for a given configuration and flow Reynolds number, and the slender body potential flow solution then obtained. The body rotation affects the solution through the position of the separation lines, which are assumed to form the junction of the feeding vortex sheets. In slender body theory, the flow over the body depends on finding the velocity potential in each cross flow plane which satisfies the boundary conditions in that plane. In the cross flow plane the junction of the feeding vortex sheets with the body will be stagnation points. Their location and the axial distance at which flow separates must be obtained either from experiment or from empirical formulation for each Reynolds number, body incidence and spin rate. The axial distance at which the vortices become well defined is known to move forwards along the body as the angle of incidence increases. The effect of spin rate on boundary layer separation is very complex.

At moderate to high angles of incidence, the effect of vortices on the flow field can be evaluated for the different sources of force. First, the position and the strength of all vortices in the cross flow plane of the body are calculated and used to estimate the corresponding potentia forces and moments using Lagally's theorem. In this case the effects of viscosity are ignored except insofar as they control the position of separation. For the second force, the velocity field due to all vortices in the cross flow plane is calculated and in particular the velocity distribution around the body surface. The velocity outside the boundary layer is thus known and the boundary layer characteristics can be determined. The distortion of the boundary layer due to the external flow field enables the force and moment on the new aerodynamic shape to be

In this second method allowance is made both for the effects of the boundary layer and for the separated vortices. A hybrid method is used in the present work. The accuracy of the results depends critically on obtaining a complete set of experimental data to cover a given range of Reynolds number, angle of attack, spin rate and body fineness ratio. Only a modest amount of such data is generally available.

III.3 Mathematical Model:

The model described and illustrated in fig. (III.1) where Γ_1 and Γ_2 are the vortex strengths located at Z_1 and Z_2. The separation angles are ψ_1 and ψ_2. The complex potential in the cross flow plane is given by:

$$F = U \sin\alpha \left(Z + \frac{a^2}{Z}\right) + \frac{i\Gamma_1}{2\pi}\left(\ln(Z - Z_1) - \ln\left(Z - \frac{a^2}{\bar{Z}_1}\right) + \ln Z\right) + \frac{i\Gamma_2}{2\pi}\left(\ln(Z - Z_2) - \ln\left(Z - \frac{a^2}{\bar{Z}_2}\right) + \ln Z\right) \qquad \text{(III.1)}$$

where Z, Z_1 and Z_2 are complex coordinates

Γ_1, Γ_2 are positive whenever the circulation is clockwise.

The complex velocity F is given by:

$$\frac{dF}{dZ} = U \sin\alpha \left(1 - \frac{a^2}{Z^2}\right) + \frac{i\Gamma_1}{2\pi}\left(\frac{1}{Z - Z_1} - \frac{1}{Z - \frac{a^2}{\bar{Z}_1}} + \frac{1}{Z}\right) + \frac{i\Gamma_2}{2\pi}\left(\frac{1}{Z - Z_2} - \frac{1}{Z - \frac{a^2}{\bar{Z}_2}} + \frac{1}{Z}\right) \qquad \text{(III.2)}$$

where $\bar{Z}_1$ and $\bar{Z}_2$ are complex conjugates.

The vortices are considered to be fed from the points s_1 and s_2 on the body surface where the flow separates away from the body. The vortex strength at a given location is determined from the condition that the fluid velocity vanishes at the separation points and is defined by

$$\left(\frac{dF}{dz}\right)_{s_1, s_2} = 0 \qquad \text{(III.3)}$$

Equation (III.3) yields two equations in Γ_1 and Γ_2 after substitution using equation (III.2), with the vortex locations and separation positions derived from experimental data [3]. These vortex core locations were obtained by probing the wake of the cylinder using a Keil tube. The position of the minimum total pressure was identified as the centre of the vortex cores. The cross flow separation positions were measured by means of a hot wire anemometer with its axis parallel to the cylinder axis. For a symmetric wake development of a non rotating circular cylinder, the vortex strength Γ was expressed [16] as a function of axial distance and the angle of incidence at Mach number M = .1 as

$$\frac{\Gamma}{2\pi Ua} = 0.14\,\alpha^2\, x/a \qquad \text{(III.4)}$$

For the asymmetric case, the following form is sought for the vortex strengths:-

$$\frac{\Gamma_i}{2\pi Ua} = a_i\,\alpha^2\,\frac{x}{a}\left(1 + b_i\,\bar{\omega} + c_i\,\bar{\omega}^2 + \ldots\right)$$

$$i = 1,2 \qquad \text{(III.5)}$$

where a_i, b_i, c_i are constants depending on the flow conditions, R_n and M. Analysis of further experimental data [1,3] yields:-

$$\frac{\Gamma_1}{2\pi Ua} = 0.115\,\alpha^2\, x/a\,(1.0 + 1.65\bar{\omega} + 0.95\,\bar{\omega}^2 + \ldots) \qquad \text{(III.6)}$$

$$\frac{\Gamma_2}{2\pi Ua} = -0.115\alpha^2 \, x/a(1.0 \mp 1.5\,\bar{\omega} + 1.15\,\bar{\omega}^2 + \ldots) \qquad \text{(III.7)}$$

valid over a range of R_n from $6 \cdot 10^4$ to $2 \cdot 10^5$; based on body diameter and free stream velocity.* The circumferential velocity distribution using equation (III.2) is illustrated roughly in fig. (III.3), which can be considered in three distinct regions. The first region is on the windward side of the cylinder between the forward stagnation point and the separation point s_2. The second region lies between s_1 and s_2 in the leeward side of the cylinder. Lastly there is the region between s_1 and the forward stagnation point. The velocity distribution is given by the following equation

$$\begin{aligned}
\bar{w} &= \alpha\, d_1 \sin\pi \frac{\theta - \theta_o}{\psi_1 - \theta_o} && \text{for } \theta_o < \theta < \psi_1 \\
&= \alpha\, d_2 \sin 2\pi \frac{\theta - \psi_1}{\psi_2 - \psi_1} && \text{for } \psi_1 < \theta < \psi_2 \\
&= \alpha\, d_3 \sin\pi \frac{\theta - \psi_2}{2\pi + \theta_o - \psi_2} && \text{for } \psi_2 < \theta < 2\pi + \theta_o
\end{aligned} \qquad \text{(III.8)}$$

where d_1, d_2 and d_3 are obtained from equation (III.2) for a particular axial station and they are described more fully in Appendix B.

Neglecting any pressure changes along the body axis, equation (III.8) is used with the appropriate boundary conditions to solve the boundary layer equations (II.4) for each of the regions. The details of the solution are presented in Appendix B together with the numerical values of the perturbation functions. The boundary layer characteristics are obtained in the same way as described in Appendix C.

---

* Equations (III.6) and (III.7) are empirical fits and do not exactly satisfy $b_2 = -b_1$ and $c_1 = c_2$. However, the resultant numerical error in the Magnus coefficients is small.

CHAPTER IV

Magnus Effect

IV.1 Method of Analysis:

The evaluation of Magnus force and its moment involves contributions from different sources. The boundary layer displacement thickness asymmetry arises from the angle of incidence and spin rate combination. A radial pressure gradient is formed by the centrifugal force acting within the boundary layer. The skin friction and the circulation distribution also provide contributions to the Magnus force and moment.

The asymmetry of the boundary layer displacement thickness distribution with respect to the angle of incidence plane produces a side force component. This force is calculated by solving the inviscid flow about a new surface resulting from adding the displacement thickness at the body surface. This is the major contribution to the Magnus force and moment whenever the angle of incidence and spin rate are small enough to ensure a boundary layer attached to the body surface over its whole length. It then represents 70 - 80% of the total Magnus force. The second contribution arises from the surface shear stress which is also an asymmetric function and its integration over the whole cylinder surface provides an additional term in the total Magnus force. According to the calculations, this term is about 5% of the total Magnus force. Another contribution is that due to the radial pressure gradient through the boundary layer thickness. It arises from the centrifugal action in the boundary layer flow. The radial pressure asymmetry, with respect to the angle of incidence plane, adds about 15 - 25% to the total Magnus force. The final and most complicated term which contributes to Magnus force and

moment results from the free vorticity. The effect of circulation increases with increase in incidence having negligible effect for attached flow conditions. Whenever separation takes place, the standing vortices dominate the contribution to Magnus force. It will be shown here that, at high angles of incidence, the asymmetric orientation of the separated vortices is the source of a large part of the total Magnus force. Consequently the boundary layer displacement thickness contribution to Magnus effect may then be neglected. The vortex strengths build up due to the vorticity shed into the wake in the cross flow plane. The existence of vorticity in the flow field modifies the pressure distribution in the inviscid flow and will modify the boundary layer characteristics.

IV.2 Magnus Effect Formulation:

The major contribution to Magnus force and moment is due to the normal pressure distribution asymmetry. The effective aerodynamic shape will consist of the original shape and the boundary layer displacement thickness distorted by body rotation. The velocity potential of the cross flow plane at any station along the body axis is given by

$$\Phi = \phi_i + \phi \qquad \text{(IV.1)}$$

where ϕ_i is the inviscid potential and ϕ is the perturbation potential due to the displacement thickness. Assuming $\frac{\partial^2 \phi}{\partial x^2}$ is a small quantity, the perturbation potential will satisfy the two dimensional Laplace equation $\nabla^2 \phi = 0$ at any station x. The boundary conditions are $\left.\frac{\partial \phi}{\partial y}\right|_{y=\infty} = 0$ and $\left.\frac{\partial \phi}{\partial y}\right|_{y=0} = U \frac{\partial \Delta}{\partial x}$ where $\frac{\partial \Delta}{\partial x}$ is the slope of the effective body shape.† The required solution for the perturbation potential at the surface can

†The cross flow component in the surface velocity condition has not been included because the resultant ϕ component does not contribute to the Magnus force.

be shown to include the term (see Appendix C, section C.3).

$$\phi = -Ua \frac{d\Lambda_s}{dx} \sin(\frac{z}{a}) \qquad (IV.2)$$

where Δ_s is the amplitude of the sin(z/a) component of the displacement thickness Δ.

The pressure coefficient neglecting second order terms is given by

$$c_p = -\frac{2}{U} \frac{\partial \phi}{\partial x}$$

and hence at the surface (a is constant with x)

$$c_p = 2a \frac{\partial^2 \Lambda}{\partial x^2} \qquad (IV.3)$$

The only terms which contribute to Magnus force are the sin(z/a) ones and, the Magnus force component is given by

$$F_{ml} = - \int_0^{\ell} \int_0^{2\pi} a\, q_\infty\, c_p \sin(z/a)\, d(z/a)\, dx \qquad (IV.4)$$

The Magnus moment coefficient referrring to the body leading edge is given by

$$M_{ml} = - \int_0^{\ell} \int_0^{2\pi} a\, q_\infty\, c_p\, x \sin(z/a)\, d(z/a)\, dx \qquad (IV.5)$$

Substituting equations (II.10) and (IV.3) into equations (IV.4) and (IV.5), the Magnus force and moment coefficients reduces to

$$K_{fl} = \sqrt{\frac{\nu}{U\ell}} \{ 5\, \alpha\, \overline{\omega} (\frac{\ell}{a})^2 (F_2 - 0.4H_o) + 9\, \alpha\, \overline{\omega}^3 (\frac{\ell}{a})^4 . (F_7 - \frac{2}{9} H_3) \} \qquad (IV.6)$$

$$K_{ml} = \sqrt{\frac{\nu}{U\ell}} \{ 3\, \alpha\, \overline{\omega} (\frac{\ell}{a})^3 (F_2 - 0.4H_o) + 7\, \alpha\, \overline{\omega}^3 (\frac{\ell}{a})^4 (F_7 - 0.222H_3) \} \qquad (IV.7)$$

F_{ml} and M_{ml} represent the major contribution to Magnus force and moment.

The radial pressure gradient is given by

$$\frac{1}{\rho} \frac{\partial p}{\partial y} = - \frac{W^2}{a} \qquad (IV.8)$$

Equations (IV.3) and (IV.8) can be used to produce a modified surface pressure coefficient in the form:-

$$C_p = 2a \frac{\partial^2 \Delta}{\partial x^2} - \frac{2}{aU^2} \int_o^\infty W^2 \, dy \qquad \text{(IV.8a)}$$

The extra force component due to the radial pressure gradient term, after substituting from (II.6) into (IV.8a), is given by

$$F_{m2} = 4 q_\infty \pi a^2 \sqrt{\frac{\nu}{U\ell}} \left(\frac{\ell}{a}\right)^2 \left(\frac{2}{3} \alpha \bar{\omega}^{-2} I_o + \frac{2}{7} \alpha \bar{\omega}^{-3} \left(\frac{\ell}{a}\right)^2 I_2 \right) \qquad \text{(IV.9)}$$

where

$$I_o = \int_o^\infty h_o'(\eta) \, (1 - f_o'(\eta)) \, d\eta$$

and

$$I_2 = \int_o^\infty h_2 (\eta) \, (1 - f_o'(\eta)) \, d\eta$$

The force and moment coefficients are given by

$$K_{f2} = \sqrt{\frac{\nu}{U\ell}} \, 2 \alpha \bar{\omega} \left(\frac{\ell}{a}\right)^2 \left[\frac{2}{3} I_o + \frac{4}{7} I_2 \bar{\omega}^{-2} \left(\frac{\ell}{a}\right)^2 \right] \qquad \text{(IV.10)}$$

and

$$K_{m2} = \sqrt{\frac{\nu}{U\ell}} \, 2 \alpha \bar{\omega} \left(\frac{\ell}{a}\right)^3 \left[\frac{4}{5} I_o + \frac{4}{9} I_2 \bar{\omega}^{-2} \left(\frac{\ell}{a}\right)^2 \right] \qquad \text{(IV.11)}$$

The third component of the Magnus force is that due to skin friction, which is given by

$$\tau = \mu \left(\frac{\partial w}{\partial y} \right)_{y=o} \qquad \text{(IV.12)}$$

The force and moment coefficients are obtained by integrating the appropriate component of τ after substituting for w:-

$$K_{f3} = \sqrt{\frac{\nu}{U\ell}} \left[\frac{4}{3} \alpha \bar{\omega} \left(\frac{\ell}{a}\right)^2 h_o' + \frac{4}{9} \alpha \bar{\omega}^{-3} \left(\frac{\ell}{a}\right)^4 h_3'(o) \right] \qquad \text{(IV.13)}$$

and

$$K_{m3} = \sqrt{\frac{\nu}{U\ell}} \left[\frac{4}{5} \alpha \bar{\omega} \left(\frac{\ell}{a}\right)^3 h_o'(o) + \frac{4}{11} \alpha \bar{\omega}^3 \left(\frac{\ell}{a}\right)^5 h_3'(o) \right] \qquad \text{(IV.14)}$$

The total Magnus force and moment for small incidence and small spin parameter developing attached flow all over the length of the cylinder are given

$$K_f = \sqrt{\frac{\nu}{U\ell}} \left[5 \alpha \bar{\omega} \left(\frac{\ell}{a}\right)^2 (F_2 - .4H_o) + 9 \alpha \bar{\omega}^3 \left(\frac{\ell}{a}\right)^4 (F_7 - \frac{2}{9} H_3) \right.$$

$$+ 4 \alpha \bar{\omega} \left(\frac{\ell}{a}\right)^2 \left(\frac{2}{3} I_o + \frac{2}{7} I_2 \bar{\omega}^2 \left(\frac{\ell}{a}\right)^2\right) +$$

$$\left. \frac{4}{3} \alpha \bar{\omega} \left(\frac{\ell}{a}\right)^2 h_o'(o) + \frac{2}{9} \alpha \bar{\omega}^3 \left(\frac{\ell}{a}\right)^4 h'_3(o) \right] + \ldots$$

(IV.15)

$$K_m = \sqrt{\frac{\nu}{U\ell}} \left[3 \alpha \bar{\omega} \left(\frac{\ell}{a}\right)^3 (F_2 - .4H_o) + 7 \alpha \bar{\omega}^3 \left(\frac{\ell}{a}\right)^5 (F_7 - \frac{2}{9} H_3) \right.$$

$$+ \alpha \bar{\omega} \left(\frac{\ell}{a}\right)^3 \left(\frac{2}{5} I_o + \frac{2}{9} I_2 \bar{\omega}^2 \left(\frac{\ell}{a}\right)^2\right) +$$

$$\left. h_o'(o) \frac{4}{5} \alpha \bar{\omega} \left(\frac{\ell}{a}\right)^3 + \frac{4}{11} \alpha \bar{\omega}^3 \left(\frac{\ell}{a}\right)^5 h_3'(o) \right] + \ldots \qquad \text{(IV.16)}$$

It has already been stressed that the sources of Magnus force at large angles of incidence are different from those at small angles of incidence and are due to the existence of two skewed vortices in the cross flow plane. The vortex wake changes the whole flow field around the cylinder and consequently the forces acting on it. The mathematical model illustrated and explained in chapter III produces a Magnus force due to the resultant normal pressure distribution around the cylinder.

The Milne-Thomson circle theorem produces the complex potential solution in equation (III.1). The forces acting on a two dimensional circular cylinder in the presence of a specified number of singularities can be calculated from either the generalized Blasius or Lagally theorems. The side force component on a three dimensional body of revolution can be obtained as:-

$$F_{m4} = -\rho \int_{o}^{\ell} \sum_{i=1}^{m} \Gamma_i (U - u_i) dx \qquad (IV.17)$$

where m is the number of vortices in the flow field, Γ_i is the strength of ith vortex rotating clockwise and u_i is the velocity of the vortex i due to all the other real vortices in the flow field. Using equation (III.5), equation (IV.17) becomes

$$F_{m4} = \pi a^2 \rho U^2 \alpha^2 \left(\frac{\ell}{d}\right)^2 \sum_{i=1}^{2} a_i (1 + \bar{\omega}\, b_i + \bar{\omega}^2 c_i) \qquad (IV.18)$$

Substituting for the values of a_i, b_i and c_i from equations (III.6) and (III.7), and using $\Gamma_1 u_1 = \Gamma_2 u_2$, the Magnus force and moment coefficients due to circulation can be expressed as

$$K_{f4} = 2\alpha^2 \left(\frac{\ell}{a}\right)^3 \sum_{i=1}^{2} a_i (1 + \bar{\omega}\, b_i + \bar{\omega}^2 c_i) \qquad (IV.19)$$

and

$$K_{m4} = \frac{2}{3}\alpha^2 \left(\frac{\ell}{a}\right)^3 \sum_{i=1}^{2} a_i (1 + \bar{\omega}\, b_i + \bar{\omega}^2 c_i) \qquad (IV.20)$$

Strictly, equations(IV.15) and(IV.16) are modified at high incidence by the effect of the parameter A, introduced in equation(B.5), which is a measure of the difference between the external potential flow field in the unseparated and separated states. However, the numerical modification to Magnus force is small because the influence of the vortices exists mainly at the surface in their immediate vicinity and there is little

effect on the gross asymmetry in boundary layer growth.*

IV.3 Results and Comparison

The numerical values of the integrals can be found in Appendix A and are used to calculate the following Magnus force and moment coefficients neglecting terms of higher order as $\alpha\,\bar{\omega}^2$, then

$$K_{f1} = 13.72\sqrt{\frac{\nu}{U\ell}}\;\alpha\,\bar{\omega}\,\left(\frac{\ell}{d}\right)^2$$

$$K_{f2} = 1.77\sqrt{\frac{\nu}{U\ell}}\;\alpha\,\bar{\omega}\,\left(\frac{\ell}{d}\right)^2$$

$$K_{f3} = -.53\sqrt{\frac{\nu}{U\ell}}\;\alpha\,\bar{\omega}\,\left(\frac{\ell}{d}\right)^2$$

The numerical value of equation (IV.15) is given by

$$K_f = 14.96\sqrt{\frac{\nu}{U\ell}}\;\alpha\,\bar{\omega}\,\left(\frac{\ell}{d}\right)^2 \qquad \text{(IV.21)}$$

by including higher terms in $\bar{\omega}$ equation (IV.15) is:-

$$K_f = \sqrt{\frac{\nu}{U\ell}}\;\alpha\,\omega\,\left(\frac{\ell}{d}\right)^2\left[14.96 - 7.03\,\bar{\omega}^2\left(\frac{\ell}{d}\right)^2\right]$$

The Magnus moment coefficient expressed in equation (IV.16) is written as follows:

$$K_m = 8.99\sqrt{\frac{\nu}{U\ell}}\;\alpha\,\bar{\omega}\,\left(\frac{\ell}{d}\right)^3 \qquad \text{(IV.22)}$$

or for higher order in $\bar{\omega}$ as

$$K_m = \sqrt{\frac{\nu}{U\ell}}\;\alpha\,\bar{\omega}\,\left(\frac{\ell}{d}\right)^3\left[8.99 - 5.46\,\bar{\omega}^2\left(\frac{\ell}{d}\right)^2 + \ldots\right]$$

The centre of pressure position (measured from nose) expressed as a function of the body length is:

---

*This applies at low incidence when the vortices are weak and close to the surface, and asymmetry arises from the spin. At higher incidences, the Magnus force is dominated by the asymmetry in normal pressure distribution.

$$\bar{x}_p = \frac{K_m}{K_f} = .6 - .365\,\omega^2\left(\frac{\ell}{d}\right)^2 + \ldots$$

The evaluation of K_{f4} and K_{m4} by using equations (III.6,7) with connection to equation (IV.19,20), K_{f4} and K_{m4} are given as follows:

$$K_{f4} = \frac{0.181}{0.238}\,\alpha^2\left(\frac{\ell}{d}\right)^2 \bar{\omega}$$

and $$K_{m4} = \frac{0.121}{0.159}\,\alpha^2\left(\frac{\ell}{d}\right)^3 \bar{\omega}$$

The total Magnus force and moment coefficients including the effect of flow separation are:-

$$K_{ft} = \alpha\,\bar{\omega}\left(\frac{\ell}{d}\right)^2\left[14.96\sqrt{\frac{\nu}{U\ell}} + \frac{0.181}{0.238}\alpha + \ldots\right]$$

and $$K_{mt} = \alpha\,\bar{\omega}\left(\frac{\ell}{d}\right)^3\left[8.99\sqrt{\frac{\nu}{U\ell}} + \frac{0.121}{0.159}\alpha + \ldots\right] \qquad \text{(IV.23)}$$

The results obtained may be compared with those obtained by Martin [2] and Kelly [7] for unseparated flow:-

$$\left.\begin{aligned} \text{Martin} \quad K_f &= 10.33\sqrt{\frac{\nu}{U\ell}}\;\alpha\,\bar{\omega}\left(\frac{\ell}{d}\right)^2 \\ \text{Kelly} \quad K_f &= 12.29\sqrt{\frac{\nu}{U\ell}}\;\alpha\,\bar{\omega}\left(\frac{\ell}{d}\right)^2 \\ \text{Present work} \quad K_f &= 14.96\sqrt{\frac{\nu}{U\ell}}\;\alpha\,\bar{\omega}\left(\frac{\ell}{d}\right)^2 \end{aligned}\right\} \qquad \text{(IV.24)}$$

Equations (IV.24) show the linear behaviour of Magnus force coefficient with α and $\bar{\omega}$ for particluar ℓ/d and Reynolds number R_e. The different constants indicated in equation(IV.24)occur because, firstly, because Martin [2] neglected the effect of both skin friction and the radial pressure gradient on Magnus force and, secondly , the present work has been carried out

using a better numerical technique (four points Runge-Kutta) as well as more accurate computing facilities.

For comparison with the theoretical results in equations (IV.21) and (IV.23), measurements of Magnus force were taken from two sources[3,17]. In the first, a conventional wind tunnel with mechanical sting support was used, in the second[17], a magnetic system was employed to support the model without aerodynamic interference. Since the use of magnetic suspension for Magnus measurements is so novel, it was felt desirable to give a brief account here of the system and the data acquisition techniques. This is contained in Appendix D and concentrates on the preliminary work with the non-spinning model to obtain the calibration constants and static aerodynamic data. The technique with the spinning model is similar[17]. The model used as the baseline for the experiments and theoretical calculations is shown in Fig.(D.1).

The detailed behaviour of Magnus force with incidence and spin ratio dependes very much on Reynolds number, tunnel flow and model surface states. A selected comparison is made here between theory and measurements to indicate the significant general points of agreement and disagreement. In Fig.(IV.1), good agreement exists at most incidences. The theory predicts that, at this spin ratio and Reynolds number, the non-linear contribution is significant at quite low angles of attack (about 3 degrees) and is dominant above 10 degrees . When the boundary layer is essentially turbulent, it is anticipated that the separation points (and hence stagnation points) will depend to a large extent only on incidence and spin ratio. The semi-empirical non-linear model will therefore give good agreement at the higher Reynolds numbers .

At reduced Reynolds number and low incidence ($<10^{o}$), the boundary layer state has an all-important effect on Magnus force as can be seen in Fig. (IV.2). Results[17] are given for a clean model and with a roughness band added on the nose shape. In both cases, negative force coefficients are present which cannot be predicted by the present theory. With the clean model, the boundary layer is essentially laminar although there is a possibility of laminar separation and turbulent reattachment. The theoretical prediction shows poor agreement over the incidence range covered (0^{o} to 7^{o}) indicating that the simple attached boundary layer model is not applicable. When an attempt is made artificially to increase the turbulence level, then the negative Magnus force mechanism at very low incidence is greatly reduced and the theory shows good agreement at incidences greater than 4^{o}. At typical full scale Reynolds numbers it is expected that the theory for the non-linear part of the Magnus force will show reasonable agreement at moderate and high incidences, because the empirical data on which the theory relies will be less sensitive to Reynolds number. The availability and analysis of interference free data over a wide range of Reynolds numbers is required to justify this in full. At low incidence, the small Magnus force present will be less sensitive to features such as laminar separation and reattachment (which is one mechanism for a negative Magnus force) but will remain sensitive to detailed base shape. The present laminar boundary layer theory for the linear part of the Magnus force is not adequate to deal with the low incidence range but the method should be capable of extension to the turbulent case.

CHAPTER V

Conclusions

The prediction of the Magnus force of the spinning circular cylinder has been studied by many people. Martin[2] and Kelly[7] predicted for the spinning body a linear variation of Magnus force with both spin rate and angle of incidence. This prediction is applicable only for a very small incidence and a low spin rate. At large incidence, the flow separates and standing vortices form to produce the non-linear behaviour of the Magnus force as illustrated in Fig.(IV.1). A method has been developed here to predict this behaviour and the results show good agreement with the experimental data. Accurate wind tunnel measurements are very difficult to obtain, since the Magnus force is much smaller than the other aerodynamic forces acting on the cylider. Negative Magnus force is not predicted by the theory but measurements[17] indicate its presence at low incidences, low Reynolds numbers and low spin ratios. The magnetic suspension balance results[17] are presented in Fig.(IV.2) and compared with the non-linear theory.

This study of Magnus force production has led to the following conclusions:-

1. The effect of the boundary layer displacement thickness is dominant only whilst the flow is attached to the body surface, i.e. for small α and ω.

2. The contribution to Magnus force from the extra asymmetry in boundary layer displacement thickness caused by the vortices in the

outer inviscid flow is much smaller than that due to the normal pressure distribution or the spin effect when the flow is unseparated.

3. The vortices developed in the inviscid outer flow from vorticity shed in the wake of the cylindrical body at angles of incidence greater than 4^{o}.

4. At large angles of attack the Magnus force is produced largely by the normal pressure distribution associated with the asymmetric potential flow field of the standing vortices.

5. More experimental work is required especially in flow visualization at small angles and in the measurements of separation positions and vortex locations.

The major limitations of the method used are:-

1. Negative Magnus forces cannot be predicted at any incidence, Reynolds number or spin ratio.

2. The model uses the assumption that the cross-flow stagnation points coincide with the separation points.

3. The method is semi-empirical in that measured positions of separation points are required.

However, agreement between predicted and measured overall Magnus forces is good, particularly at the higher incidences.

The contribution of the present work towards the prediction of Magnus forces may be summarised as:-

a. An extension of the attached flow contribution to include higher order terms in incidence and spin ratio.

b. The development of a semi-empirical non-linear method for the contribution of separated flow vortices at, moderate to high incidences.

References

1. Fletcher, C.A. "Investigation of the Magnus characteristics of spinning inclined ogive cylinder body at M = .2" WRE TN HSA 159 Oct. 1969.

2. Martin, J.C. "On Magnus effect caused by the boundary layer displacement thickness on bodies of revolution at small angle of attack". BRL Rept. No.870 1965 and J. of Aero. Sc. Vol.24 p.421 1957.

3. Fletcher, C.A. "The Magnus characteristics of a spinning body at subcritical R_n in incompressible flow" WRE. TN. 423 June 1971.

4. Martin, J.M. "Experimental correlation between the flow and Magnus characteristics of a spinning ogive nose cylinder body". AIAA. Vol.11 No.7 p.901 1973.

5. Magnus, G. "On the derivation of projectile on a remarkable phenomenon of rotating bodies". Royal Academy Vol. I part IV 1852.

6. Platou, A.S. "Magnus characteristics of finned and nonfinned projectile". AIAA. Vol.3 No.1 p.83 1965.

7. Kelly, H.R. "An analytical method for predicting the Magnus force and moment on spinning projectile" NAVORD TM 1634 1954.

8. Kelly, H.R. & Thacker "The effect of high spin on the Magnus force on a cylinder at small angle of attack". NAVORD Rept. 5036 1956.

9. Power, H.L. "Magnus effect on spinning bodies of revolution". Ph.D. thesis Iowa State University 1972.

10. Moore, F.K. "Displacement effect of a 3-D boundary layer". NACA T.N. 2722 1952.

11. Allen & Perkins "A study of the effect of viscosity on flow over slender body of revolution" NACA Rept. 1048 1951.

12. Kelly, H.R. "The estimation of normal force, drag and pitching moment coefficients for blunt based bodies of revolution at large angle of attack". J. of Aero. Sc. Vol.21 p.549 1954.

13. Buford, W.E. "Magnus effect in the case of rotating cylinder and shell" B.R.L. Rept. No.821 1954.

14. Bryson, A. "Supersonic Magnus characteristics on a finned missile" AIAA. Vol.2 No.1 p.153, 1964.

15. Thomson & Harrison "The spacing, position and strength of vortices in the wake of slender cylindrical body" WRE. No.25 June 1969.

16. Fiechter, M. "On the vortex system of high fineness ratio bodies of revolution and their influence on the aerodynamic coefficients". Tech. translation by W. Oberkamp, Notre Dame University USA.

17. R.I. Henderson "Measurements of Magnus force on a spinning projectile, including the influence of base geometry". Contract final report prepared for RARDE, 1975.

18. "Second international symposium of Electro Magnetic Suspension" July 1971 University of Southampton.

19. Brown, C.E. & Stewartson "Laminar separation" Annual Review of fluid mechanics vol. 1 1969

20. Mangler K.W. and Smith J.H.B. "A theory of the flow past a slender delta wing with leading edge separation" proceeding of Royal Soc. Series A vol. 251, P.200 1959

Bibliography

Adams, M.C. "Leading edge separation from delta wing at supersonic speeds" J.A.Sc. vol.20, p.430, 1953.

Aken & Kelly "The Magnus force on a spinning cylinder" NAVORD Rept. 712 Inst. of Aero. Sc. 1957.

Asher & Dasenjh "An experimental investigation of the formation and flow characteristics of an impulsively generated vortex street" ASME Tran. Series D Dec. 1968.

Backla, H.M. & Auchterlainie "The Magnus or Robin effect on rotating spheres" J. of fluid mechanics vol.47, Part 3, 1971.

Batchelor, G.K. "Introduction to fluid dynamics" 1970.

Betz, A. "The Magnus effect" NASA T.M. 310 1925.

Blotter, F.G. "Finite difference method of solution of boundary layer equations" AIAA Vol.8 no.2 1970.

Brown, C.E. & Stewartson "Laminar separation" Annual Review of fluid mechanics vol.1 1969.

Brown, C.E. & Michael, W.H. "On slender delta wing with leading edge separation" NACA T.N. 3830 1935.

Bryson, "Symmetric vortex separation on circular cylinders and cones" ASME of applied mechanics p.643 1959.

Carman, J.B. & Usolton, J.C. "A study of the Magnus effect on sounding rocket at supersonic speeds" J. of Spacecraft and rocket, vol.8 p.28, 1971.

Ohen, C.F. "Vortex shedding from circular cylinder in an oscillating free stream" AIAA Vol.9 p.340 1971.

Cheng, H.K. "Aerodynamics for rectangular plate with vortex separation in supersonic flow" J. Aero. Sc. vol.22 p.217, 1955.

Chu, S.T. "The compressible laminar boundary layer on a rotating body of revolution" J. of Aero. Sc. vol.21, p.345 1954.

Clack, B.L. "Navier-Stokes equations solutions for laminar incompressible flow over yawed spinning body of revolution" AIAA paper 72-112.

Clark, W.H. "Occurrence and inhibition of large yawing moments during high incidence flight of slender missile configuration" AIAA paper 72-968.

Davies "Aerodynamics of golf balls" J. of applied physics vol.20 no.9, p.821 1949.

Dor, J. "A study of general 3-D boundary layer problem in an exact numerical methods" AIAA vol.9 no.7 1971 p.1297.

Dufoult, R. & Henshow "Potential flow characteristics for arbitrary axisymmetric bodies" National Research Council of Canada, Aero. Rept. LR-556 1971.

Duncan, Thom and Young "Mechanics of fluid" Second edition 1970.

Edwards, R.H. "Leading edge separation from delta wings" J. Aero. Sc. vol.21 p.134, 1954.

Fletcher, C.A. "An explanation of the negative Magnus side force experienced by a spinning inclined ogive cylinder" W.R.E. T.N. 489 Nov. 1971.

Fox, J. "Separation studies for the similar laminar boundary layer" AIAA vol.8 no.4 p.780, 1970.

Fox, J. "Boundary layer on a rotating sphere and axisymmetric shapes" NASA T.N. 2491 1964.

Froberg, C.E. "Introduction to numerical analysis" 1970.

Funuya R. & Nakamara "Velocity profiles in the skewed boundary layer on rotating bodies" J. of applied mechanics p.17, 1970.

Gadd "Investigation of laminar separation of supersonic speed" J. Aero. Sc. vol.24 p.759, Oct. 1957.

Gasta, M. "Vortex shedding from circular cylinder at low Reynolds number" J. of fluid mechanics vol. 46 p.749 1971.

Glouat, M.B. "The flow past a rapidly rotating cylinder" J. of Royal Soc. vol. 242 series 4 1954.

Goldstein, S. "Modern development in fluid mechanics" Vol. I and II 1965.

Goodyer, M.J. "The magnetic suspension of wind tunnel models for dynamic testing" Ph.D. thesis Southampton University 1968 (U.K).

Gowen & Perkins "A study of the effect of body shape on vortex wakes at M = 2" NACA R.M. A 53IA Dec. 1953.

Greense, J.E. "A summary of experimental characteristics of a 7-5 calibre body of revolution at subsonic through supersonic speeds" NAVORD Rept. 6110 1958.

Griffith & Ma "Differential boundary layer separation effects in the flow over a rotating cylinder" Royal Aero. Soc. P.524, 1969.

Howarth, L. "Note on the boundary layer separation effects in the flow over a rotating sphere" Phill. Mag. vol.XLII No.42, 1951, p.1309.

Illingworth, C.R. "Boundary layer growth on spinning body" Phill. Mag. vol.45 p.1 1954.

Iverson, J.D. "Correlation of Magnus force data for slender spinning cylinder" AIAA paper 72-966.

Jacobson, I.D. "Influence of boundary layer transition on Magnus force on a spinning body of revolution" Ph.D. thesis Virginia Univ. June 1970.

Jacobson, I.D. "Magnus characteristics of arbitrary rotating bodies" School of engineering and applied science, University of Virginia, U.S.A.

Kelly, H.R. "The Magnus effect at high Rn" J. Aero. Sc. 1956.

Kelly, H.R. & Thacker "The effect of high spin on the Magnus force on a cylinder at small angle of attack" NAVORD Rept. 5036 1956.

Krahn, E. "Negative Magnus force" J. of Aero. Sc. vol.25, p.377 1956.

Kuhn, C.D. & Spevngler, S. "Theoretical analysis of vortex shedding from bodies of revolution in motion" AIAA vol.9 no.5 1971 p.784.

Lamb, H. "Hydrodynamics" 1932.

Mangler & Smith "A theory of the flow past a slender delta wing with leading edge separation" Proceeding of Royal Soc. Series A vol.251, p.200 1959.

Mello, J.F. "Investigation of normal force distribution and wake vortex characteristic of bodies of revolution at supersonic speeds" J. Aero. Sc. vol.26, no.3, 1959.

Moore, F.K. "Laminar boundary layer on cone in supersonic flow at large angle of attack" NACA Rept. 1132, 1953.

Mosinskis, G.J. "Calculation of separation points in incompressible turbulent flows" J. of aircraft p.618, vol.9 no.9.

Muraco, R.J. "The laminar boundary layer on a spinning body of revolution" AIAA paper 70-1377, 1970.

Oberkampt, W.L. "Aerodynamics of finned missile at high angle of attack" Ph.D. thesis, Univ. of Notre Dame, Aug. 1970.

Pipes, L.A. & Havvill, L.R. "Applied mathematics for engineers and physicists".

Prandtl, L. "Application of the Magnus coefficient to the wind propulsion of ships" NACA T.M. 367 1924.

Regan, F.J. "Magnus effect" AGARD CP-10 1966.

Reding, J.P. "Nonexistence of axisymmetric separated flow" AIAA vol.7 no.7 p.1374, 1969.

Sarpkaya, T. "An analytical study of separated flow about circular cylinder" ASME Basic engineering Dec.'68.

Sarpkaya, T. "Separated flow about lifting bodies and impulsive flow about cylinder" AIAA vol.4 no.3 1966.

Sarparkaya, T. "An analytical study of separated flow about circular cylinder" ASME Basic Engng 1968.

Sarparkaya, T. "Lift, drag and added mass coefficient for circular cylinder immersed in a time dependent flow" ASME Series D 1963 p.13.

Sarparkaya,T. & Gorrison "Vortex formation and resistance in unsteady flow" ASME Series D 1963.

Sohindel, L.H. "Effect of vortex separation on the lift distribution on bodies of elliptic cross section" J. of aircraft vol.6 no.6 1969.

Schlichting, H. "Boundary layer theory" 1962.

Seath, D. "Equilibrium vortex position" J. of Space craft and Rocket vol.8 no.1 p.72, 1971.

Smith, J.H. "Improved calculation of leading edge separation for slender delta wing" T.R 66070 R.A.E. 1966.

Sturck, W.B. "Boundary layer studies on a spinning cone" AIAA paper no.72-967 1972.

Swanson, W.M. "An experimental investigation of the Magnus effect" OOR Project no. 1082 1956.

Swanson, W.M. "The Magnus effect: a summary of investigation to date" ASME Basic Engng 1961.

Tinling, B.E. & Allen, C.Q. "An investigation of the normal force and vortex wake characteristics of an ogive cylinder body at subsonic speeds" NASA T.N. D1297, 1962.

Tritton, D.J. "A note on vortex streets behind circular cylinder at low Rn" J. fluid mechanics vol.43, p.203, 1971.

Vaugh, H.R. & George, O.C. "Surface flow angles on an ogive cylinder at angle of attack at supersonic speeds" Sandia Lab. SC-RR-70-081 Dec. '71.

Vaugh, H.R. & George "The characteristics of laminar boundary layer on a spinning tangent ogive cylinder at angle of attack" SC-RR-71-085 1972.

Vaugh, H.R. & Reis "A Magnus theory for bodies of revolution" SC-RR-72-0537, 1973.

Wang, K.C. "Separation patterns of boundary layer over an inclined body of revolution" AIAA, vol.10 no.8 1972.

Appendix A

Solution of Boundary Layer Equations with Laminar Flow.

The three dimensional boundary layer equations (A.1) for semi-infinite circular cylinder using the Cartesian coordinate system illustrated in fig. (II.1) are given by

$$\left.\begin{aligned} u\frac{\partial u}{\partial x} + v\frac{\partial u}{\partial y} + w\frac{\partial u}{\partial z} &= -\frac{1}{\rho}\frac{\partial P}{\partial x} + \nu\frac{\partial^2 u}{\partial y^2} \\ u\frac{\partial w}{\partial x} + v\frac{\partial w}{\partial y} + w\frac{\partial w}{\partial z} &= -\frac{1}{\rho}\frac{\partial P}{\partial z} + \nu\frac{\partial^2 w}{\partial y^2} \\ \frac{\partial P}{\partial y} &= 0 \\ \frac{\partial u}{\partial x} + \frac{\partial v}{\partial y} + \frac{\partial w}{\partial z} &= 0 \end{aligned}\right\} \qquad (A.1)$$

The boundary layer characteristics are obtained by solving equations (A.1) whilst satisfying the following boundary conditions:-

$$u = v = 0 \quad \text{and } w = \omega a \quad \text{at } y = 0$$

$$u = U\cos\alpha \quad \text{and } w = 2U\sin\alpha\,(z/a) \quad \text{at } y = \infty$$

For small angles of incidence such that $\sin\alpha \approx \alpha$ and $\cos\alpha \approx 1 - \alpha^2/2$, the above boundary conditions reduce to

$$u = U(1 - \alpha^2/2) \text{ and } w = 2U\alpha\sin(z/a) \text{ at } y = \infty$$

The pressure gradients are given by

$$\frac{\partial P}{\partial x} = 0$$

$$\text{and } \frac{\partial P}{\partial z} = -4\alpha^2\frac{\rho U^2}{a}\sin(z/a)\cos(z/a)$$

It is assumed that the velocity profiles in the boundary layer may be expressed as following

$$\left.\begin{aligned} \bar{u} &= u_o + u_1 + u_2 + u_3 + u_4 + \cdots \\ \bar{v} &= v_o + v_1 + v_2 + v_3 + v_4 + \cdots \\ \bar{w} &= w_1 + w_2 + w_3 + w_4 + \cdots \end{aligned}\right\} \qquad (A.2)$$

where $\bar{u}$, $\bar{v}$ and $\bar{w}$ are velocities non-dimensionalised with respect to the free stream velocity U. u_o, v_o are the non-dimensional velocity components for zero spin and zero incidence and the subscripts 1,2,3,4 refer to the perturbations in the first, second, third and fourth order in α and/or $\bar{\omega}$. The boundary layer equations for the zero order perturbation are given by:-

$$\left.\begin{aligned} u_o \frac{\partial u_o}{\partial y} + v_o \frac{\partial u_o}{\partial y} &= \frac{\nu}{U} \frac{\partial^2 u_o}{\partial y^2} \\ \frac{\partial u_o}{\partial x} + \frac{\partial v_o}{\partial y} &= 0 \end{aligned}\right\} \qquad (A.3)$$

Assuming a stream function ψ as follows

$$\psi = \sqrt{\nu U x}\ f_o(\eta)$$

where

$$\eta = \frac{y}{x}\sqrt{\frac{Ux}{\nu}}$$

The velocity components are

$$\left.\begin{aligned} u_o &= f_o'(\eta) \\ \text{and} \quad v_o &= \tfrac{1}{2}\sqrt{\frac{\nu}{Ux}}\ (\eta f_o'(\eta) - f_o(\eta)) \end{aligned}\right\} \qquad (A.4)$$

The boundary conditions are $u_o = v_o = 0$ at $y = 0$ and $u_o = 1$ at $y = \infty$. Substituting equations (A.4) into (A.3) results in an ordinary differential equation in the function $f_o(\eta)$ as following

$$f_o'''(\eta) = -\tfrac{1}{2} f_o(\eta)\, f_o''(\eta) \qquad (A.5)$$

The solution to equation (A.5) must satisfy the boundary conditions $f_o(o) = f_o'(o) = 0$ and $f_o'(\infty) = 1$.

The boundary layer equations for the first order perturbation in α or ω is given by

$$\left.\begin{aligned} u_o \frac{\partial u_1}{\partial x} + u_1 \frac{\partial u_o}{\partial x} + v_o \frac{\partial u_1}{\partial y} + v_1 \frac{\partial u_o}{\partial y} &= \frac{\nu}{U} \frac{\partial^2 u_1}{\partial y^2} \\ u_o \frac{\partial w_1}{\partial x} + v_o \frac{\partial w_1}{\partial y} &= \frac{\nu}{U} \frac{\partial^2 w_1}{\partial y^2} \\ \frac{\partial u_1}{\partial x} + \frac{\partial v_1}{\partial y} + \frac{\partial w_1}{\partial z} &= 0 \end{aligned}\right\} \qquad (A.6)$$

The velocity profiles take the forms given below

$$\left.\begin{aligned} u_1 &= \frac{\alpha x}{a} f_1(\eta) \cos(z/a) \\ v_1 &= \sqrt{\frac{\nu}{Ux}}\, \frac{\alpha x}{a}\, g_o(\eta) \cos(z/a) \\ w_1 &= \bar{\omega}(1 - f_o'(\eta)) + 2\alpha f_o'(\eta) \sin(z/a) \end{aligned}\right\} \qquad (A.7)$$

where $u_1 = v_1 = 0$ and $w_1 = \bar{\omega}$ at $y = 0$ and

$u_1 = 0$ and $w_1 = 2\alpha \sin(z/a)$ at $y = \infty$

This leads to $f_1(o) = g_o(o) = 0$ and $f_1(\infty) = 0$.

Substituting equation (A.7) into (A.6) gives two simultaneous ordinary differential equations in $f_1(\eta)$ and $g_o(\eta)$ as follows:-

$$f_1''(\eta) = f_o'(\eta)\, f_1(\eta) - \tfrac{1}{2} f_1'(\eta)\, f_o(\eta) + f_o''(\eta)\,(g_o(\eta) - \frac{\eta}{2} f_1(\eta))$$

$$g_o'(\eta) = \frac{\eta}{2} f_1'(\eta) - f_1(\eta) - 2 f_o'(\eta) \qquad \text{(A.8)}$$

The second order perturbation in α ω or α^2 leads to the boundary layer equations:-

$$u_o \frac{\partial u_2}{\partial x} + v_o \frac{\partial u_2}{\partial y} + u_1 \frac{\partial u_1}{\partial x} + v_1 \frac{\partial u_1}{\partial y} + u_2 \frac{\partial u_o}{\partial y} + v_2 \frac{\partial u_o}{\partial x} + w_1 \frac{\partial u_1}{\partial z} = \frac{\nu}{U} \frac{\partial^2 u_2}{\partial y^2}$$

$$u_o \frac{\partial w_2}{\partial x} + u_1 \frac{\partial w_1}{\partial x} + v_1 \frac{\partial w_1}{\partial y} + v_o \frac{\partial w_2}{\partial y} + w_1 \frac{\partial w_1}{\partial z} = \frac{1}{\rho} \frac{\partial P}{\partial z} + \frac{\nu}{U} \frac{\partial^2 w_2}{\partial y^2}$$

$$\frac{\partial u_2}{\partial x} + \frac{\partial u_2}{\partial y} + \frac{\partial w_2}{\partial z} = 0 \qquad \text{(A.9)}$$

Appropriate forms for the velocity profile in the boundary layer are given by:-

$$u_2 = \alpha \bar{\omega} \left(\frac{x}{a}\right)^2 f_2(\eta) \sin(z/a) + \alpha^2 \left(\frac{x}{a}\right)^2 (f_3(\eta) + f_4(\eta) \cos(z/a)) - \frac{\alpha^2}{2} f_5'(\eta)$$

$$v_2 = \sqrt{\frac{\nu}{Ux}} \{ \alpha \bar{\omega} \left(\frac{x}{a}\right)^2 g_1(\eta) \sin(z/a) + \alpha^2 \left(\frac{x}{a}\right)^2 (g_2(\eta) + g_3(\eta) \cos(z/a)) - \frac{\alpha^2}{4} (\eta f_5'(\eta) - f_5(\eta)) \}$$

and

$$w_2 = \alpha \bar{\omega} \frac{x}{a} h_o(\eta) \cos(z/a) + (\alpha^2 x/a)\, h_1(\eta) \sin(2z/a) \qquad \text{(A.10)}$$

where $u_2 = v_2 = w_2 = 0$ at $y = 0$ and

$$u_2 = -\frac{\alpha^2}{2} \quad \text{and} \quad w_2 = 0 \quad \text{at } y = \infty$$

The above boundary conditions lead to the following,

$$h_o(o) = h_o(\infty) = 0 \quad \text{and} \quad h_1(o) = h_1(\infty) = 0$$

$$f_2(o) = g_1(o) = 0 \quad \text{and} \quad f_2(\infty) = 0$$

$$f_3(o) = g_2(o) = 0 \quad \text{and} \quad f_3(\infty) = 0$$

$$f_4(o) = g_3(o) = 0 \quad \text{and} \quad f_4(\infty) = 0$$

$$\text{and} \quad f_5(o) = f_5'(o) = 0 \quad \text{and} \quad f_5'(\infty) = 1$$

Substituting equations (A.10) into (A.7) gives a set of ordinary differential equations in f_2, f_3, f_4, f_5, as follows:-

$$h_o''(\eta) = f_o'(\eta)\, h_o(\eta) - \tfrac{1}{2} h_o'(\eta)\, f_o(\eta) + f_o''(\eta)\left(\frac{\eta}{2} f_1(\eta) - g_o(\eta)\right) + 2 f_o'(\eta)\,(1 - f_o'(\eta)) \qquad (A.11)$$

$$\left.\begin{aligned} f_2''(\eta) &= 2f_2(\eta)\, f_o'(\eta) - \tfrac{1}{2} f_o(\eta)\, f_2'(\eta) + f_o'(\eta)\left(g_1(\eta) - \frac{\eta}{2} f_2(\eta)\right) - \\ &\quad f_1(\eta)(1 - f_o'(\eta)) \\ g_1'(\eta) &= \frac{\eta}{2} f_2'(\eta) - 2f_2(\eta) + h_o(\eta) \end{aligned}\right\} \qquad (A.12)$$

$$h_1''(\eta) = f_o'(\eta)\, h_1(\eta) - \tfrac{1}{2} h_1'(\eta)\, f_o(\eta) + 2(f_o'^2(\eta) - 1) + f_o''(\eta)\left(\frac{\eta}{2} f_1(\eta) - g_o(\eta)\right) \qquad (A.13)$$

$$\left.\begin{aligned} f_3''(\eta) &= 2f_3(\eta)\, f_o'(\eta) - \tfrac{1}{2} f_o(\eta)\, f_3'(\eta) + f_o''(\eta)\left(g_2(\eta) - \frac{\eta}{2} f_3(\eta)\right) \\ &\quad + \tfrac{1}{2} g_o(\eta)\, f_1'(\eta) - f_o'(\eta)\, f_1(\eta) \\ &\quad + \tfrac{1}{2} f_1(\eta)\left(f_1(\eta) - \frac{\eta}{2} f_1'(\eta)\right) \\ g_2'(\eta) &= \frac{\eta}{2} f_3'(\eta) - 2 f_3(\eta) \end{aligned}\right\} \qquad (A.14)$$

$$f_4''(\eta) = 2f_4(\eta)\, f_o'(\eta) - \tfrac{1}{2} f_o(\eta)\, f_4'(\eta) + f_o''(\eta)\left(g_3(\eta) - \frac{\eta}{2} f_4(\eta)\right) + \tfrac{1}{2} f_1(\eta)\left(f_1(\eta) - \frac{\eta}{2} f_1'(\eta)\right) + \tfrac{1}{2} g_o(\eta)\, f_1'(\eta) + \tfrac{1}{2} f_o'(\eta)\, f_1(\eta)$$

$$g_3(\eta) = \frac{\eta}{2} f_4'(\eta) - 2 f_4(\eta) - 2 h_1(\eta) \qquad \text{(A.15)}$$

and

$$2f_5''' + f_o(\eta)\, f_5''(\eta) + f_5(\eta)\, f_o''(\eta) = 0 \qquad \text{(A.16)}$$

The perturbation of order $\alpha\, \bar{\omega}^2$ yields the boundary layer equations:-

$$u_o \frac{\partial u_3}{\partial x} + u_3 \frac{\partial u_o}{\partial x} + v_o \frac{\partial u_3}{\partial y} + v_3 \frac{\partial u_o}{\partial y} + w_1 \frac{\partial u_2}{\partial z} = \frac{\nu}{U} \frac{\partial^2 u_3}{\partial y^2}$$

$$u_o \frac{\partial w_3}{\partial x} + u_2 \frac{\partial w_1}{\partial x} + v_o \frac{\partial w_3}{\partial y} + v_2 \frac{\partial w_1}{\partial y} + w_1 \frac{\partial w_2}{\partial y} = \frac{\nu}{U} \frac{\partial^2 w_3}{\partial y^2}$$

$$\frac{\partial u_3}{\partial x} + \frac{\partial v_3}{\partial y} + \frac{\partial w_3}{\partial z} = 0 \qquad \text{(A.17)}$$

The following are appropriate forms for the velocity profiles in the boundary layer.

$$u_3 = \alpha\, \bar{\omega}^2 \left(\frac{x}{a}\right)^3 f_5(\eta) \cos(z/a)$$

$$v_3 = \sqrt{\frac{\nu}{Ux}}\, \omega\, \bar{\omega}^2 \left(\frac{x}{a}\right)^3 g_5(\eta) \cos(z/a) \qquad \text{(A.18)}$$

$$w_3 = \alpha\, \bar{\omega}^2 \left(\frac{x}{a}\right)^2 h_2(\eta) \sin(z/a)$$

where $u_3 = v_3 = w_3 = 0$ at $y = 0$ and

$u_3 = w_3 = 0$ at $y = \infty$

This yields $f_6(o) = g_5(o) = 0$ and $f_5(\infty) = 0$ and $h_2(o) = h_2(\infty) = 0$

Substituting equations (A.18) into (A.17) gives the following ordinary differential equations

$$h_2''(\eta) = 2\, h_2(\eta)\, f_o'(\eta)\, h_2'(\eta) + f_o''(\eta)\left(-g_1(\eta) + \frac{\eta}{2} f_2(\eta)\right) - h_o(\eta)(1 - f_o'(\eta)) \qquad (A.19)$$

and

$$\left.\begin{aligned} f_6''(\eta) &= 3\, f_6(\eta)\, f_o'(\eta) - \tfrac{1}{2} f_o(\eta)\, f_6'(\eta) + \frac{\eta}{2} f_o''(\eta)\, f_o(\eta) \\ &\quad + g_5(\eta)\, f_o''(\eta) + f_2(\eta)(1 - f_o'(\eta)) \\ g_5'(\eta) &= \frac{\eta}{2} f_6'(\eta) - 3\, f_6(\eta) - h_2(\eta) \end{aligned}\right\} \qquad (A.20)$$

Consideration of perturbation quantities of order $\alpha\, \bar{\omega}^3$ leads to the boundary layer equations:-

$$\left.\begin{aligned} u_o \frac{\partial u_4}{\partial x} + u_4 \frac{\partial u_6}{\partial x} + v_o \frac{\partial u_4}{\partial y} + v_4 \frac{\partial u_6}{\partial y} + w_1 \frac{\partial u_3}{\partial z} &= \frac{\nu}{U} \frac{\partial^2 u_4}{\partial y^2} \\ u_o \frac{\partial u_4}{\partial x} + v_o \frac{\partial w_4}{\partial y} + u_3 \frac{\partial w_1}{\partial x} + v_3 \frac{\partial w_1}{\partial y} + w_1 \frac{\partial w_3}{\partial z} &= \frac{\nu}{U} \frac{\partial^2 w_4}{\partial y^2} \\ \frac{\partial u_4}{\partial x} + \frac{\partial v_4}{\partial y} + \frac{\partial w_4}{\partial z} &= 0 \end{aligned}\right\} \qquad (A.21)$$

The required boundary conditions to be satisfied are:-

$$\left.\begin{aligned} u_4 &= \alpha\, \bar{\omega}^3 \left(\frac{x}{a}\right)^4 f_7(\eta) \sin(z/a) \\ v_4 &= \sqrt{\frac{\nu}{Ux}}\, \alpha\, \bar{\omega}^3 \left(\frac{x}{a}\right)^4 g_6(\eta) \sin(z/a) \\ \text{and } w_4 &= \alpha\, \bar{\omega}^3 \left(\frac{x}{a}\right)^3 h_3(\eta) \cos(z/a) \end{aligned}\right\} \qquad (A.22)$$

where $u_4 = v_4 = w_4 = 0$ at $y = 0$ and $u_4 = 0$ $w_4 = 0$ at $y = \infty$

The above boundary conditions yield, $f_7(o) = g_6(o) = 0$ and $f_7(\infty) = 0$, $h_3(o) = h_3(\infty) = 0$

Substituting equations (A.22) into (A.21) gives:-

$$h_3''(\eta) = 3h_3(\eta)\, f_o'(\eta) - \tfrac{1}{2} f_o(\eta)\, h_3'(\eta) - \frac{\eta}{2} f_o''(\eta)\, f_6(\eta) + g_5(\eta)\, f_o''(\eta) + h_2(\eta)(1 - f_o'(\eta)) \qquad (A.23)$$

$$\left.\begin{aligned} f_7''(\eta) &= 4 f_7(\eta)\, f_o'(\eta) - \tfrac{1}{2} f_o(\eta) f_7''(\eta) + \tfrac{\eta}{2} f_o''(\eta) f_7(\eta) + \\ &\quad g_6(\eta)\, f_o''(\eta) + f_6(\eta)(1 - f_o'(\eta)) \\ g_6'(\eta) &= \frac{\eta}{2} f_7'(\eta) - 4 f_7(\eta) + h_3(\eta) \end{aligned}\right\} \qquad (A.24)$$

The total velocity profile to order 4 in the boundary layer is given by

$$\begin{aligned} \bar{u} &= f_o'(\eta) + \frac{\alpha x}{a} f_1(\eta)\, f_1(\eta) \cos(z/a) + \alpha\, \omega \left(\frac{x}{a}\right)^2 f_2(\eta) \sin(z/a) \\ &\quad + \left(\frac{\alpha x}{a}\right)^2 (f_3(\eta) + f_4(\eta) \cos(2z/a)) - \frac{\alpha^2}{2} f_5'(\eta) \\ &\quad + \alpha\, \bar{\omega}^2 \left(\frac{x}{a}\right)^3 f_6(\eta) \cos(z/a) + \alpha\, \bar{\omega}^3 \left(\frac{x}{a}\right)^4 f_7(\eta) \sin(z/a) \end{aligned}$$

$$\begin{aligned} \bar{v} &= \sqrt{\frac{\nu}{Ux}} \left\{ \tfrac{1}{2} (\eta\, f_o'(\eta) - f_o(\eta)) + \frac{\alpha x}{a} g_o(\eta) \cos(z/a) + \right. \\ &\quad \alpha\, \omega \left(\frac{x}{a}\right)^2 g_1(\eta) \sin(z/a) + \left(\frac{\alpha x}{a}\right)^2 (g_2(\eta) + g_3(\eta) \cos(2z/a)) \\ &\quad - \frac{\alpha^2}{4} (\eta\, f_5'(\eta) - f_5(\eta)) + \alpha\, \bar{\omega}^2 \left(\frac{x}{a}\right)^3 g_5(\eta) \cos(z/a) + \alpha\, \bar{\omega}^3 \left(\frac{x}{a}\right)^4 \\ &\quad \left. g_6(\eta) \sin(z/a) \right\} + \ldots \end{aligned}$$

and

$$\bar{w} = \bar{\omega}(1 - f_o'(\eta)) + 2\alpha f_o'(\eta) \sin(z/a) + \alpha \bar{\omega}(\frac{x}{a}) h_o(\eta) \cos(z/a)$$
$$+ \alpha^2 \frac{x}{a} h_1(\eta) \sin(2z/a) + \alpha \bar{\omega}^2 (\frac{x}{a})^2 h_2(\eta) \sin(z/a) +$$
$$\alpha \bar{\omega}^3 (\frac{x}{a})^3 h_3(\eta) \cos(z/a) + \ldots \qquad (A.25)$$

The velocity components in the boundary layer are functions of the perturbation function f_n, g_n and h_n.

The perturbation function equations (A.5), (A.8), (A.11) through (A.16), (A.19),(A.20) and (A.23,24) were solved numerically by digital computer using the ICL standard routines F4RUNK. This routine solves a system of first order differential equations using the Runge-Kutta four point method. It integrates the equations as an initial value problem. The boundary layer equations are, however, of the two point boundary value type. For this reason guesses of the unknown initial value are made and then the differential equations are integrated from the body surface to the edge of the boundary layer. If the conditions are not then satisfied, the initial values are adjusted and the integrations repeated. This process continues until the solutions satisfy the outer edge boundary conditions. Figures (A.7) through (A.12) show the results of these calculations. The integrals of the perturbation functions are given by

$$F_o = \int_o^\infty (1 - f_o'(\eta))d\eta = 1.72106$$

$$F_1 = \int_o^\infty f_1(\eta)\, d\eta = 1.72612$$

$$F_2 = \int_o^\infty f_2(\eta)\, d\eta = 1.486063$$

$$F_3 \int_o^\infty f_3(\eta)\, d\eta = -.269982$$

$$F_4 = \int_0^\infty f_4(\eta)\, d\eta = +3.3203$$

$$F_5 \int_0^\infty f_5'(\eta)\, d\eta = 7.87324$$

$$F_6 \int_0^\infty f_6(\eta)\, d\eta = -1.085211$$

$$F_7 \int_0^\infty f_7(\eta) = -.62773$$

$$H_o = \int_0^\infty h_o(\eta)\, d\eta = -2.7469$$

$$H_1 = \int_0^\infty h_1(\eta)\, d\eta = 4.96995$$

$$H_2 = \int_0^\infty h_2(\eta)\, d\eta = -1.8395$$

$$H_3 = \int_0^\infty h_3(\eta)\, d\eta = 1.1489$$

$$I_o = \int_0^\infty f_o'(\eta)\,(1 - f_o'(\eta))d\eta = .663836$$

$$I_2 = \int_0^\infty h_2(\eta)\,(1 - f_o'(\eta))d\eta = -.70909$$

The above integrals were evaluated using the University of Nottingham Subroutines 'NAG' D01ADF. This routine estimates the values of definite integrals using Gaussian quadratures with a specified number of points. These integrals are used in evaluating the boundary layer displacement thicknesses and also the Magnus force. The following values are also required for the evaluation of the skin friction,

$h_o'(o) = -.794160$

$h_2'(o) = .430109$

Appendix B

The Solution of the Boundary Layer Equations including the Effect of Vortices

The three dimensional boundary layer equations for the semi-infinite circular cylinder using a Cartesian coordinate system have been derived in Appendix A. The boundary layer characteristics were obtained by solving the boundary layer equations and satisfying the boundary conditions on the body surface and at the inviscid outer flow obtained from slender body theory. For the model of the standing vortices discussed in the Introduction, a similar approach to the boundary layer calculation as in Appendix A is possible because the vortices are assumed to lie well outside the viscous layer and therefore result only in a modification to the external potential flow field. Whilst a simplified representation of the true flow, it does afford an analytic mathematical form capable of predicting closely the type of streamline flow observed on bodies of revolution at moderate incidences. Such streamline flow is consistent with the assumption that the potential cross-flow stagnation points coincide with the real separation points. Cross-flow velocity components tend to be small compared with the free stream velocity even in the presence of the vortices and the boundary layer growth remains dominated by the axi-symmetric zero order contribution, except in the immediate vicinity of the separation lines. Since the main contribution to the Magnus force at moderate to high incidence is shown to arise from the normal pressure distribution produced by vortex asymmetry, it is felt that little error results from neglecting details of flow in the

region of separation. Using the mathematical model illustrated in fig. (III.1), the complex potential in the cross flow plane can be obtained in the form:-

$$F = U \alpha \left(Z + \frac{a^2}{Z}\right) + \frac{i\Gamma_1}{2\pi}\left(\ln(Z - Z_1) - \ln\left(Z - \frac{a^2}{\bar{Z}_1}\right) + \ln Z\right)$$

$$+ \frac{i\Gamma_2}{2\pi}\left(\ln(Z - Z_2) - \ln\left(Z - \frac{a^2}{\bar{Z}_1}\right) + \ln Z\right) \qquad \text{(B.1)}$$

The vortex strength is positive rotating clockwise.

The complex velocity is given by

$$\frac{dF}{dZ} = U\alpha\left(1 - \frac{a^2}{Z^2}\right) + \frac{i\Gamma_1}{2\pi}\left(\frac{1}{Z - Z_1} - \frac{1}{Z - \frac{a^2}{\bar{Z}_1}} + \frac{1}{Z}\right)$$

$$+ \frac{i\Gamma_2}{2\pi}\left(\frac{1}{Z - Z_2} - \frac{1}{Z - \frac{a^2}{\bar{Z}_2}} + \frac{1}{Z}\right) \qquad \text{(B.2)}$$

The vortices Γ_1 and Γ_2 are considered to be fed from the separation points s_1 and s_2 on the body surface. The vortex strength at a given vortex location is determined from the condition that the velocity at the separation points vanishes.

$$\left.\frac{dr}{dz}\right|_{s_1, s_2} = 0 \qquad (B.3)$$

Equation (B.3) supplies two equations in Γ_1 and Γ_2 which may be solved by an iterative method. The velocity distribution can be expressed

$$\bar{w} = \alpha\, d_1 \sin \pi \frac{\theta - \theta_o}{\psi_1 - \theta_o} \qquad \text{for } \theta_o < \theta < \psi_1$$

$$= \alpha\, d_2 \sin \pi \frac{\theta - \psi_1}{\psi_2 - \psi_1} \qquad \text{for } \psi_1 < \theta < \psi_2 \qquad (B.\ )$$

$$= \alpha\, d_3 \sin \pi \frac{\theta - \psi_2}{2\pi + \theta_o - \psi_2} \qquad \text{for } \psi_2 < \theta < 2\pi + \theta_o$$

where d_1 is the value of $\bar{w}$ evaluated at $\theta = \psi_1 + \theta_o/2$ etc. The general form for $\bar{w}$ is expressed as

$$\bar{w} = w(\theta)$$

The required solution of the boundary layer equations uses the boundary conditions $u = v = 0$ and $w = \omega a$ on the body surface and $u = U(1 - \alpha^2/2)$ and $w = \bar{w} U$ at the edge of the boundary layer. A non dimensional function is assumed in the form:-

$$A = w(\theta)/(\alpha \sin(\theta)) \qquad (B.5)$$

Neglecting the axial pressure gradient $\frac{\partial P}{\partial x}$, the same procedure is used as in Appendix A to obtain the perturbation functions in different orders in α or/ $\bar{\omega}$ as:-

$$f_o(\eta)\, f_o''(\eta) + 2\, f_o'''(\eta) = 0 \qquad (B.6)$$

with the boundary conditions $f_o(o) = f_o'(o) = 0$ and $f_o'(\infty) = 1$.

$$f_1''(\eta) = f_o'(\eta)\, f_1(\eta) - \tfrac{1}{2} f_1'(\eta)\, f_o(\eta) - \frac{\eta}{2} f_o''(\eta)\, f_1(\eta) + g_o(\eta)\, f_o''(\eta)$$

$$g_o'(\eta) = \frac{\eta}{2} f_1'(\eta) - f_1(\eta) - f_o'(\eta) \qquad \text{(B.7)}$$

with the boundary conditions $f_1(o) = f_o(o) = 0$ and $f_1'(\infty) = 0$.

$$h_o''(\eta) = f_o'(\eta)\, h_o(\eta) - \tfrac{1}{2} f_o(\eta)\, h_o'(\eta) + \frac{\eta}{2} f_1(\eta)\, f_o''(\eta)$$

$$- f_o''(\eta)\, f_o(\eta) + f_o'(\eta)(1 - f_o'(\eta)) \qquad \text{(B.8)}$$

with $h_o(o) = h_o(\infty) = 0$.

$$h_1(\eta) = f_o'(\eta)\, h_1(\eta) - \tfrac{1}{2} f_o(\eta)\, h_1'(\eta) - \frac{\eta}{4} f_o''(\eta)\, f_1(\eta) - \tfrac{1}{2}$$

$$+ \tfrac{1}{2} f_1'^{2}(\eta) - \tfrac{1}{2} g_o(\eta)\, f_o''(\eta) \qquad \text{(B.9)}$$

and $h_1(o) = h_1(\infty) = 0$

$$f_2''(\eta) = 2 f_2(\eta)\, f_o'(\eta) + f_o''(\eta)(g_1(\eta) - \frac{\eta}{2} f_2(\eta)) - .5\, f_o(\eta)$$

$$f_2'(\eta) - f_1(\eta)(1 - f_o'(\eta))$$

$$g_1'(\eta) = \frac{\eta}{2} f_2'(\eta) - 2 f_2(\eta) + h_o(\eta) \qquad \text{(B.10)}$$

where $f_2(o) = f_2(\infty) = g_1(o) = 0$

$$f_3''(\eta) = 2 f_3(\eta)\, f_o'(\eta) - \tfrac{1}{2} f_o(\eta)\, f_3'(\eta) - \frac{\eta}{2} f_o''(\eta)\, f_3(\eta) +$$

$$f_o''(\eta)\, g_2(\eta) + \tfrac{1}{2} g_o(\eta)\, f_1'(\eta) + \tfrac{1}{2} f_o'(\eta)\, f_1(\eta) +$$

$$\tfrac{1}{2} f_1(\eta)(f_1(\eta) - \frac{\eta}{2} f_1'(\eta))$$

$$g_2'(\eta) = \frac{\eta}{2} f_3'(\eta) - 2 f_3(\eta) \qquad \text{(B.11)}$$

with the appropriate boundary conditions $f_3(o) = g_2(o) = f_3(\infty) = 0$

$$\left.\begin{aligned} f_4''(\eta) &= 2 f_4(\eta) f_o'(\eta) - \tfrac{1}{2} f_4'(\eta) f_o(\eta) - \frac{\eta}{2} f_o''(\eta) f_4(\eta) \\ &\quad + \tfrac{1}{2} f_1(\eta)(f_1(\eta) - \frac{\eta}{2} f_1'(\eta)) + \tfrac{1}{2} g_o(\eta) f_o'(\eta) \\ &\quad + g_3(\eta) f_o''(\eta) + \tfrac{1}{2} f_1(\eta) f_o'(\eta) \\ g_3(\eta) &= \frac{\eta}{2} f_4'(\eta) - 2 f_4(\eta) - 2 h_1(\eta) \end{aligned}\right\} \quad (B.12)$$

where

$$f_4(o) = g_3(o) = 0 \text{ and } f_4(\infty) = 0$$

$$2f_5'''(\eta) + f_o(\eta) f_5''(\eta) + f_5(\eta) f_o''(\eta) = 0 \quad (B.13)$$

with

$$f_5(o) = f_5'(o) = 0 \quad \text{and} \quad f_5'(\infty) = 1$$

$$h_2''(\eta) = 2 f_o'(\eta) h_2(\eta) - \tfrac{1}{2} f_o(\eta) h_2'(\eta) + \frac{\eta}{2} f_o''(\eta) f_2(\eta) - g_1(\eta) f_o''(\eta) - h_o(\eta)(1 - f_o'(\eta)) \quad (B.14)$$

and $h_2(o) = h_2(\infty) = 0$

$$\left.\begin{aligned} f_6''(\eta) &= 3 f_6(\eta) f_o'(\eta) - \tfrac{1}{2} f_o(\eta) f_6'(\eta) + \frac{\eta}{2} f_o''(\eta) f_o(\eta) \\ &\quad + g_5(\eta) f_o''(\eta) + f_2(\eta)(1 - f_o''(\eta) \\ g_5'(\eta) &= \frac{\eta}{2} f_6'(\eta) - 3 f_6(\eta) - h_2(\eta) \end{aligned}\right\} \quad (B.15)$$

where

$$f_6(o) = g_5(o) = 0 \text{ and } f_6(\infty) = 0$$

$$h_3''(\eta) = 3 h_3(\eta) f_o'(\eta) - \tfrac{1}{2} h_3'(\eta) f_o(\eta) - \frac{\eta}{2} f_o''(\eta) + f_6(\eta) + g_5(\eta) f_o''(\eta) + h_2(\eta)(1 - f_o'(\eta)) \quad (B.16)$$

where

$$h_3(o) = h_3(\infty) = 0$$

and

$$f_7'(\eta) = 4 f_7(\eta) f_o'(\eta) - \tfrac{1}{2} f_7'(\eta) f_o(\eta) + \frac{\eta}{2} f_o''(\eta) f_7(\eta) + g_6(\eta) f_o''(\eta) + f_6(\eta)(1 - f_o'(\eta))$$

$$g_6'(\eta) = \frac{\eta}{2} f_7'(\eta) - 4 f_7(\eta) + h_3(\eta) \qquad \text{(B.17)}$$

with the boundary conditions

$$f_7(o) = g_6(o) = 0 \text{ and } f_7(\infty) = 0$$

where $\eta = \frac{y}{x}\sqrt{\frac{Ux}{\nu}}$

Equations (b.6) through (B.17) are ordinary differential equations in f_n, g_n and h_n similar to those described in Appendix A. The velocity components in the boundary layer are given by:-

$$\bar{u} = f_o'(\eta) + \frac{\alpha x}{a} A \cos\Theta f_1(\eta) + \alpha \bar{\omega} \left(\frac{x}{a}\right)^2 A f_2(\eta) \sin\Theta + \alpha^2 \left(\frac{x}{a}\right)^2 A^2 (f_3(\eta) + f_4(\eta) \cos(2\Theta)) - \frac{\alpha^2}{2} f_5'(\eta) + \alpha \bar{\omega}^2 \left(\frac{x}{a}\right)^3 A f_6(\eta) + \alpha \bar{\omega}^3 \left(\frac{x}{a}\right)^4 A f_7(\eta) \sin\Theta$$

$$\bar{v} = \sqrt{\frac{\nu}{Ux}} \left\{ \tfrac{1}{2}(\eta f_o'(\eta) - f_o(\eta)) + \frac{\alpha x}{a} A g_o(\eta) \cos\Theta + \alpha \bar{\omega} \left(\frac{x}{a}\right)^2 A g_1(\eta) \sin\Theta + \left(\frac{\alpha x}{a}\right)^2 A^2 (g_2(\eta) + g_3(\eta) \cos 2\Theta) - \frac{\alpha^2}{4} (\eta f_5'(\eta) - f_5(\eta)) + \alpha \bar{\omega}^2 \left(\frac{x}{a}\right)^3 A g_5(\omega) \cos\Theta + \alpha \bar{\omega}^3 \left(\frac{x}{a}\right)^4 A g_6(\eta) \right\} + \ldots$$

and

$$\bar{w} = \bar{\omega}(1 - f_o'(\eta)) + \alpha A f_o'(\eta) \sin\Theta + \alpha \bar{\omega} \frac{x}{a} A h_o(\eta) \cos\Theta +$$

$$\alpha^2 \frac{x}{a} A^2 h_1(\eta) \sin 2\Theta + \alpha \bar{\omega}^2 \left(\frac{x}{a}\right)^2 A h_2(\eta) \sin\Theta +$$

$$\alpha \bar{\omega}^3 \left(\frac{x}{a}\right)^3 A h_3(\eta) \cos\Theta \qquad (B.18)$$

where

$\Theta = z/a$ and A is evaluated from equation (B.5)

The perturbation functions have similar behaviour to those mentioned in Appendix A. The numerical values of the integrals are given by:-

$$F_o = \int_o^\infty (1 - f_o'(\eta))\, d\eta = 1.72016$$

$$F_1 = \int_o^\infty f_1(\eta)\, d\eta = -.86306$$

$$F_2 = \int_o^\infty f_2(\eta)\, d\eta = .773063$$

$$F_3 = \int_o^\infty f_3(\eta)\, d\eta = +.299221$$

$$F_4 = \int_o^\infty f_4(\eta)\, d\eta = -1.596147$$

$$F_5 = \int_o^\infty f_5'(\eta)\, d\eta = 7.87329$$

$$F_6 = \int_o^\infty f_6(\eta)\, d\eta = -.524311$$

$$F_7 = \int_0^\infty f_7(\eta)\, d\eta = -.311284$$

$$H_o = \int_0^\infty h_o(\eta)\, d\eta = -1.02114$$

$$H_1 = \int_0^\infty h_1(\eta)\, d\eta = 1.2939085$$

$$H_2 = \int_0^\infty h_2(\eta)\, d\eta = -.799268$$

$$H_3 = \int_0^\infty h_3(\eta)\, d\eta = .539085$$

$$I_o = \int_0^\infty f_o'(\eta)(1 - f_o'(\eta)) = .66383$$

$$I_2 = \int_0^\infty h_2(\eta)(1 - f_o'(\eta) = -.3012703$$

The numerical values of the above integrals have been estimated in the same way as described in Appendix A, and the values of

$$h_o'(o) = -.312781$$

$$h_3'(o) = .190277$$

will be required in estimating the skin friction.

Appendix C

Boundary Layer Displacement Thickness

C.1 Method of derivation

Moore [10] has derived an expression for the calculation of the boundary layer displacement thickness for the three dimensional flow over a non rotating surface. It has been suggested [10] that this expression is also valid for rotating surfaces. The solution of the boundary layer equations yields a certain velocity distribution $v(x,z)$ normal to the body surface at the outer edge $h(x,z)$ of the boundary layer. Outside the boundary layer the flow is assumed inviscid. If $\underline{q}$ is the velocity vector given by

$$\underline{q} = \underline{i}u + \underline{j}v + \underline{k}w \qquad (C.1)$$

where

$\underline{i}$, $\underline{j}$ and $\underline{k}$ are the unit vector in x, y and z directions respectively.

Assume $y = \Delta(x,z)$ is a fictitious impermeable surface which, in a completely inviscid flow, would produce a velocity V_n (normal to the real surface) at $y = h(x,z)$ equal to the normal velocity component V_b which exists as a result of the boundary layer presence. The velocities V_b and V_n are related by:-

$$V_b = \underline{q} \cdot \text{grad}\, \Delta + (h - \Delta) \left(\frac{\partial V_n}{\partial y}\right)_{y=o} \qquad (C.2)$$

The mass flow defects are given by

$$\frac{\partial \rho v}{\partial y} = -\frac{\partial \rho u}{\partial x} - \frac{\partial \rho w}{\partial z} \qquad (C.3)$$

At y = h, the equation (C.3) becomes

$$\rho V_b = -\int_o^h \left[\frac{\partial(\rho u)}{\partial x} + \frac{\partial(\rho w)}{\partial z} \right] dy \qquad (C.4)$$

If the flow is incompressible (ρ = constant) equations (C.2) through (C.4), using Cartesian coordinate, gives

$$\frac{\partial}{\partial x}(\Lambda - \delta_x) + \frac{\partial}{\partial z} \frac{w_p}{U_p} (\Lambda - \delta_z) = 0 \qquad (C.5)$$

where

$$\delta_x = \int_o^\delta \left(1 - \frac{u}{U_p}\right) dy$$

$$\delta_z = \int_o^\delta \left(1 - \frac{w}{w_p}\right) dy \qquad (C.6)$$

$$u_p = U(1 - \alpha^2/2)$$

and $$w_p = 2U\,\alpha \sin(z/a)$$

C.2 Method of analysis:

The evaluation of the boundary layer displacement thickness Δ depends on the solution of the boundary layer equations. This solution has been explained in Appendix A. It is assumed that the displacement thickness could be given by

$$\Delta = \Delta_o + \Delta_1 + \Delta_2 + \Delta_3 + \Delta_4 + \cdots \qquad (C.7)$$

where the subscripts denote the order of the perturbation quantities in

$\bar{\omega}$ and/or α. Δ_o is the displacement thickness for zero spin and zero incidence. Substituting for the velocity profile equations into (C.6), δ_x and δ_z become:

$$\delta_x = \sqrt{\frac{\nu x}{U}} \Big\{ F_o - \frac{\alpha x}{a} F_1 \cos(z/a) - \alpha \bar{\omega} \left(\frac{x}{a}\right)^2 F_2 \sin(z/a) - \alpha \bar{\omega}^2 \left(\frac{x}{a}\right)^3 F_6 \cos(z/a) - \alpha \bar{\omega}^3 \left(\frac{x}{a}\right)^4 F_7 \sin(z/a) - \alpha^2 \left(\frac{x}{a}\right)^2 (F_3 - F_4 \cos(2z/a)) + \frac{\alpha^2}{2}(F_5 - \eta + F_o) \Big\} + \ldots$$

and

$$\delta_z = \sqrt{\frac{\nu x}{U}} \Big\{ F_o - \frac{\bar{\omega}}{2\alpha \sin(z/a)} F_o - \tfrac{1}{2} \bar{\omega} \frac{x}{a} \cos(z/a) H_o - \tfrac{1}{2} \bar{\omega}^2 \left(\frac{x}{a}\right)^2 \sin(z/a) H_2 - \frac{\alpha}{2} \frac{x}{a} \cos(z/a) H_1 - \tfrac{1}{2} \bar{\omega}^3 \left(\frac{x}{a}\right)^3 \cot(z/a) H_3 \Big\} + \ldots \qquad (C.9)$$

Substituting equations (C.6) through (C.9) into (C.5) gives a system of partial differential equations of successive orders in the perturbation quantities $\bar{\omega}$ and α :-

$$\frac{\partial}{\partial x}\left(\Delta_o - \sqrt{\frac{\nu x}{U}} F_o\right) = 0 \qquad (C.10)$$

$$\frac{\partial}{\partial x}\left(\Delta_1 + \sqrt{\frac{\nu x}{U}} F_1 \cos(z/a)\right) + \frac{\partial}{\partial z} \sin(z/a)\left(\Delta_o - \sqrt{\frac{\nu x}{U}} F_o\right) = 0 \qquad (C.11)$$

$$\frac{\partial}{\partial x}\left(\Delta_2 + \sqrt{\frac{\nu x}{U}} \left[\alpha \omega \left(\frac{x}{a}\right)^2 F_2 \sin(z/a) + \alpha^2 \left(\frac{x}{a}\right)^2 (F_3 + F_4 \cos 2z/a) - \tfrac{1}{2}(F_5 - \eta + F_o)\right]\right) + \frac{\partial}{\partial z} 2\alpha \sin(z/a)\left(\Delta_1 + \sqrt{\frac{\nu x}{U}} \frac{\bar{\omega}}{2} \cot z/a \, H_o\right) = 0 \qquad (C.12)$$

$$\frac{\partial}{\partial x}\left[\Delta_3 + \sqrt{\frac{\nu x}{U}}\left(\alpha\,\bar{\omega}^2\left(\frac{x}{a}\right)^3 F_6\cos(z/a)\right)\right] + \frac{\partial}{\partial z}\left[2\,\alpha\,\sin(z/a)\,\left(\Delta_2 + \sqrt{\frac{\nu x}{U}}\,\frac{\bar{\omega}^2}{2}\left(\frac{x}{a}\right)^2\sin(z/a)\right)\right] = 0 \qquad (C.13)$$

and

$$\frac{\partial}{\partial x}\left[\Delta_4 + \sqrt{\frac{\nu x}{U}}\left(\alpha\,\bar{\omega}^3\left(\frac{x}{a}\right)^4 F_6\sin(z/a)\right)\right] + \frac{\partial}{\partial z}\left[2\,\alpha\,\sin(z/a)\,\left(\Delta_3 + \sqrt{\frac{\nu x}{U}}\,\frac{\bar{\omega}^3}{2}\left(\frac{x}{a}\right)^3\cot(z/a)\,H_3\right)\right] = 0 \qquad (C.14)$$

Solving equations (C.10) through (C.14) gives:-

$$\Delta_o = \sqrt{\frac{\nu x}{U}}\,F_o \qquad (C.15)$$

$$\Delta_1 = -\sqrt{\frac{\nu x}{U}}\,\frac{\alpha x}{a}\,F_1\cos(z/a) \qquad (C.16)$$

$$\Delta_2 = -\sqrt{\frac{\nu x}{U}}\left\{\alpha\,\bar{\omega}\left(\frac{x}{a}\right)^2\sin(z/a)\left(F_2 - \frac{2}{5}H_o\right) + \left(\frac{\alpha x}{a}\right)^2\left[F_3 + \left(F_4 + .4(H_1 - 2F_1)\right)\cos(2z/a)\right] - \frac{\alpha^2}{2}\left(F_5 - \eta + F_o\right)\right\} \qquad (C.17)$$

$$\Delta_3 = -\sqrt{\frac{\nu x}{U}}\left(\alpha\,\bar{\omega}^2\left(\frac{x}{a}\right)^3\left(F_6 + \frac{2}{7}H_2\right)\cos(z/a)\right) \qquad (C.18)$$

and

$$\Delta_4 = -\sqrt{\frac{\nu x}{U}}\left[\alpha\,\bar{\omega}^3\left(\frac{x}{a}\right)^4\left(F_7 - \frac{2}{9}H_3\right)\sin(z/a)\right] \qquad (C.19)$$

The displacement thickness is thus given by:

$$\Delta = \sqrt{\frac{\nu x}{U}}\left\{F_o - \frac{\alpha x}{a} F_1 \cos(z/a) - \alpha \bar{\omega}\left(\frac{x}{a}\right)^2 (F_2 - .4H_o) \sin(z/a) - \right.$$

$$(\alpha x/a)^2 (F_3 + (F_4 + .4(H_1 - 2F_1)) \sin 2z/a) + \frac{\alpha^2}{2} (F_5 - \eta + F_o) -$$

$$\left. \alpha \bar{\omega}^2 \left(\frac{x}{a}\right)^3 (F_6 + \frac{2}{9} H_2) \cos(z/a) - \alpha \bar{\omega}^3 \left(\frac{x}{a}\right)^4 (F_7 - \frac{2}{9} H_3) \sin(z/a)\right\} + \ldots$$

(C.20)

where F_o, F_1, ... H_o, H_1, ... are the integrals of the perturbation functions whose numerical values are presented in Appendices A and B.

C.3. Modified Boundary Condition and Velocity Potential

In the cross flow plane (r,ϕ) in fig. (II.1) the boundary layer displacement thickness produces an effective increment $\Delta(\phi,x)$ on the radius a of the cylindrical surface, where $\Delta << a$. The normal to the modified surface therefore makes the following small and approximate angles relative to the normal to the solid surface at the same ϕ and x:-

$$\gamma \simeq \frac{1}{a} \frac{\partial \Delta}{\partial \phi} \quad \text{in the } r\text{-}\phi \text{ plane}$$

$$\frac{\partial \Delta}{\partial x} \quad \text{in the } \phi\text{-}x \text{ plane.}$$

The normal velocity boundary condition to be satisfied by the velocity potential becomes:-

$$v_n \simeq -U \sin \alpha \cos(\phi - \gamma) + U \frac{\partial \Delta}{\partial x}$$

This can be satisfied by expanding Δ as a Fourier series in ϕ and using the velocity potential solutions in polar coordinates. In the calculation of Magnus force, it is found that only the sin ϕ part of $\frac{\partial \Delta}{\partial x}$ contributes. The corresponding part of the velocity potential is:-

$$- U \frac{a^2}{r} \frac{d\Delta_s}{dx} \sin \phi$$

where Δ_s is the amplitude of the sin ϕ term in Δ. Thus using the surface coordinate system defined in fig. (II.1), the surface velocity potential becomes:-

$$- Ua \frac{d\Delta_s}{dx} \sin\left(\frac{z}{a}\right)$$

Appendix D

Measurements of Forces and Moments on a Body of Revolution

D.1 Introduction and description of the balance

The measurement of the steady aerodynamic forces and moments on a body of revolution at incidence was performed as an initial stage towards the measurement of Magnus force [17,18] . The University of Southampton magnetic suspension balance system was used. The balance and the suspension system was built and developed in the Aeronautics department for the measurement of aerodynamic stability derivatives. However, static data can be extracted without modification of the system. The magnetic balance is used with an induced flow closed circuit tunnel, the working section having a nominal size of 8" by 6" and an atmospheric stagnation pressure. The six component magnetic balance incorporates integral feedback control so that the model remains in a fixed spatial position as the aerodynamic loads change.

D.2 Calibration and data reduction

Magnetic field interactions occur due to the simultaneous application of steady external forces and moments. Force/current and moment/current calibrations are obtained using direct application of loads for vertical forces and moments, and a system of harnesses and pulleys for the drag force. Calibrations are repeated over a range of model attitude and with different combinations of the applied loads. The model position sensors are calibrated using a jig with Vernier adjustment and positive location with respect to the working section. The currents in

the various coils can be expressed as follows:-

$$I_a = I_a(F, D, M, \alpha)$$

$$I_f = I_f(F, D, M, \alpha) \qquad (D.1)$$

$$I_d = I_d(F, D, M, \alpha)$$

where I_a, I_f and I_d are the currents in the aft, fore and drag coils respectively and F, D, M and α are the lift, drag, pitching moment and incidence respectively. Equations (D.1) can be edpanded in terms of their derivatives:-

$$\delta I_a = \frac{\partial I_a}{\partial F}\delta F + \frac{\partial I_a}{\partial D}\delta D + \frac{\partial I_a}{\partial M}\delta M + \frac{\partial I_a}{\partial \alpha}\delta\alpha + \frac{\partial^2 I_a}{\partial F^2}\delta\bar{F}^2 + \frac{\partial^2 I_a}{\partial D^2}\delta\bar{D}^2 +$$

$$\frac{\partial^2 I_a}{\partial M^2}\delta\bar{M}^2 + \frac{\partial^2 I_a}{\partial \alpha^2}\delta\bar{\alpha}^2 + \frac{\partial^2 I_a}{\partial F \partial\alpha}\delta F\delta\alpha \frac{\partial^2 I_a}{\partial D\partial\alpha}\delta D\delta\alpha + \frac{\partial^2 I_a}{\partial M\partial\alpha}\delta M\delta\alpha + \ldots$$

(D.2)

I_f and I_d can be expressed in similar way and combined in a matrix form given by:-

$$[I] = \left[[A] + \alpha [B] \right] [F] \qquad (D.3)$$

where $[I]$ and $[F]$ are column matrices, $[B]$ and $[A]$ are square matrices given by:-

$$[I] = \begin{bmatrix} I_a \\ I_f \\ I_d \end{bmatrix} \quad \text{and} \quad [F] = \begin{bmatrix} F \\ D \\ M \end{bmatrix}$$

$$[A] = \begin{bmatrix} \frac{\partial I_a}{\partial F} & \frac{\partial I_a}{\partial M} & \frac{\partial I_a}{\partial D} \\ \frac{\partial I_f}{\partial F} & \frac{\partial I_f}{\partial M} & \frac{\partial I_f}{\partial D} \\ \frac{\partial I_d}{\partial F} & \frac{\partial I_d}{\partial M} & \frac{\partial I_d}{\partial D} \end{bmatrix}$$

and

$$[B] = \begin{bmatrix} \frac{\partial^2 I_a}{\partial F \partial \alpha} & \frac{\partial^2 I_a}{\partial M \partial \alpha} & \frac{\partial^2 I_a}{\partial D \partial \alpha} \\ \frac{\partial^2 I_f}{\partial F \partial \alpha} & \frac{\partial^2 I_f}{\partial M \partial \alpha} & \frac{\partial^2 I_f}{\partial D \partial \alpha} \\ \frac{\partial^2 I_d}{\partial F \partial \alpha} & \frac{\partial^2 I_d}{\partial M \partial \alpha} & \frac{\partial^2 I_d}{\partial D \partial \alpha} \end{bmatrix}$$

The elements of $[A]$ and $[B]$ have been obtained by two different methods:-

a) point by point using a digital voltmeter readout.

b) Tape-recorded signals with subsequent digital computer analysis.

Method (a) has been used extensively. Even though digital voltmeter readout greatly simplifies the process of taking measurement, a complete calibration run is a long process. Method (b) has a shorter calibration time but requires more complicated analysis. The applied force and reading voltage whilst the moment, drag and incidence were held constant to give $\frac{\partial I_a}{\partial F}$. By putting the model at another setting and repeating the force variation, the second derivatives, such that $\frac{\partial^2 I_a}{\partial F \partial \alpha}$, were obtained. The same procedure was used to obtain all the derivatives. The numerical values for the model tested are:-

$$[A] = \begin{bmatrix} -.42 & 11.16 & 2.85 \\ 11.13 & -9.667 & -.42 \\ .95 & 3.5 & 25.5 \end{bmatrix}$$

where the units in $[A]$ are millivolts per gram and

$$[B] = \begin{bmatrix} -.08 & .13 & -.345 \\ -.07 & .104 & .19 \\ -.027 & 0 & 0 \end{bmatrix}$$

where $[B]$ is measured in millivolt/gram/degree.

The applied forces and moments are related to the currents by:-

$$[F] = \left[[A] + \alpha [B] \right]^{-1} [I] \qquad (D.4)$$

The increase of the matrix $\left[[A] + \alpha [B] \right]$ must be evaluated at each incidence α. The aerodynamic forces and moments are obtained by evaluating equation (D.4) with the elements of $[I]$ corresponding to the increments between wind-on and wind-off readings at the same incidence. The data was fed to the ICL 1907 computer to carry out the matrix arithmetic and typical results shown in figures (D.2) through (D.7).

D.3 Results and comparison

The model was a 7 calibre AN spinner, the dimensions and construction of which are shown in fig. (D.1). Tests were carried out at a tunnel Mach number of M = 0.2 and at a Reynolds number of 1.2×10^5 when based on body diameter.

The results obtained are illustrated in fig. (D.2) through (D.7). These results are in good agreement with data from conventional wind

tunnels [18] . The aerodynamic forces and pitching moment coefficients defined,

$$c_D = D/q_\infty S$$

$$c_L = L/q_\infty S$$

and $$c_M = M/q_\infty S D$$

where the moment coefficient is referring to the tail of the body.

View looking forward

Incidence α is +ve nose up

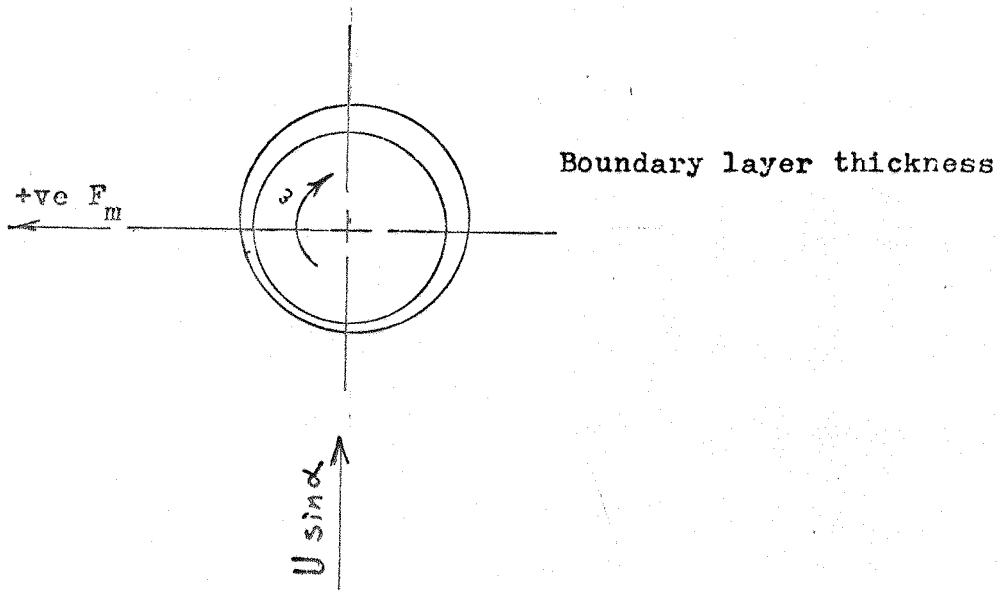

Fig(I.1) Positive direction of Magnus force.

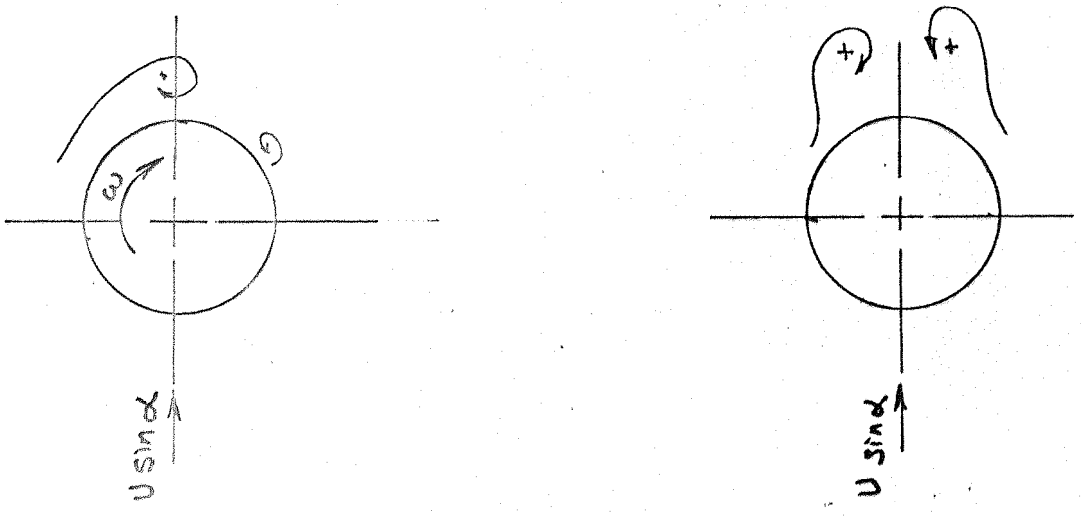

Rotating

Non-Rotating

Fig(I.2) Vortex formation for rotating and Non-rotating cylinder.

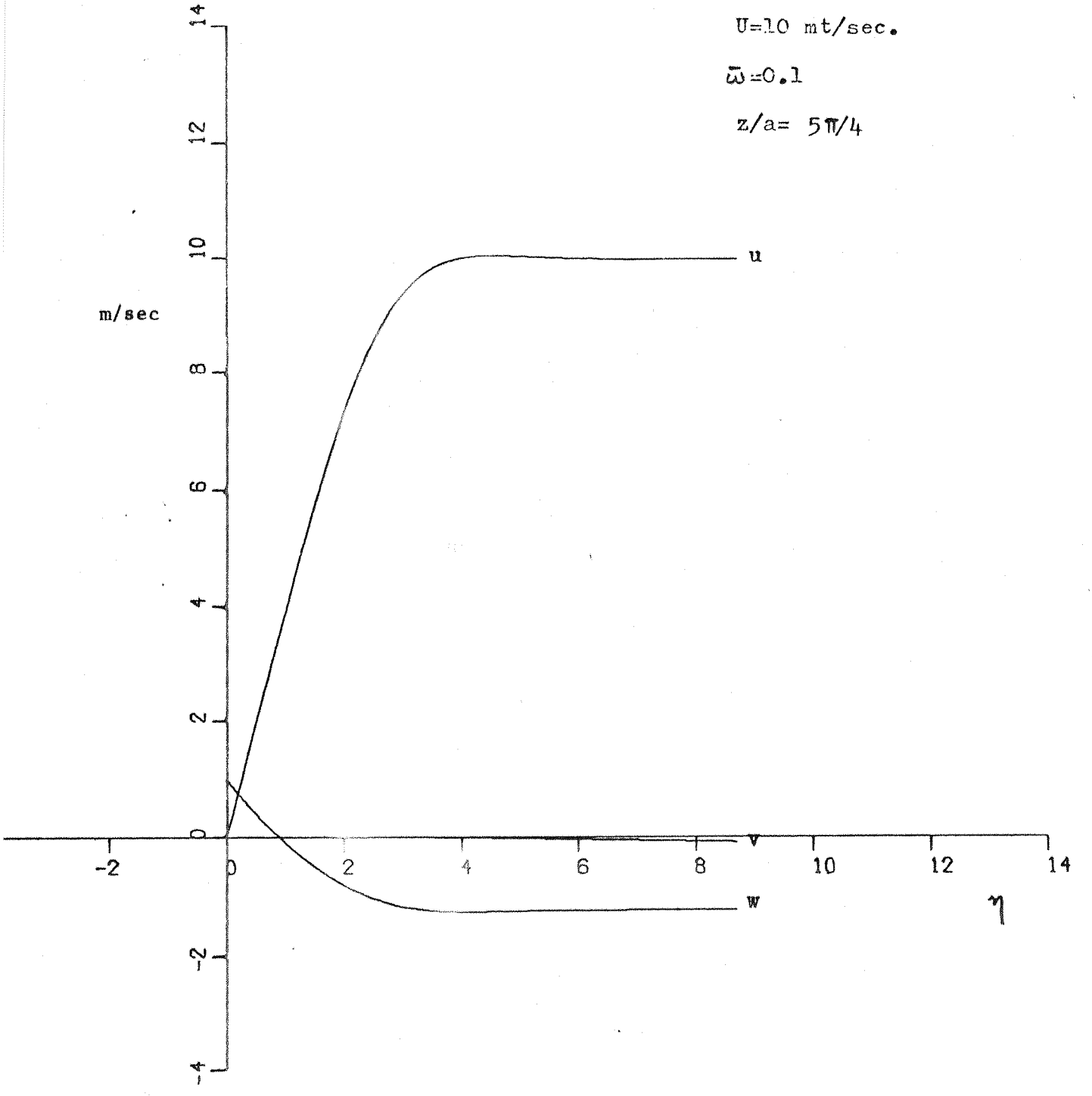

Fig(11.2) Velocity profiles of a rotating cylinder

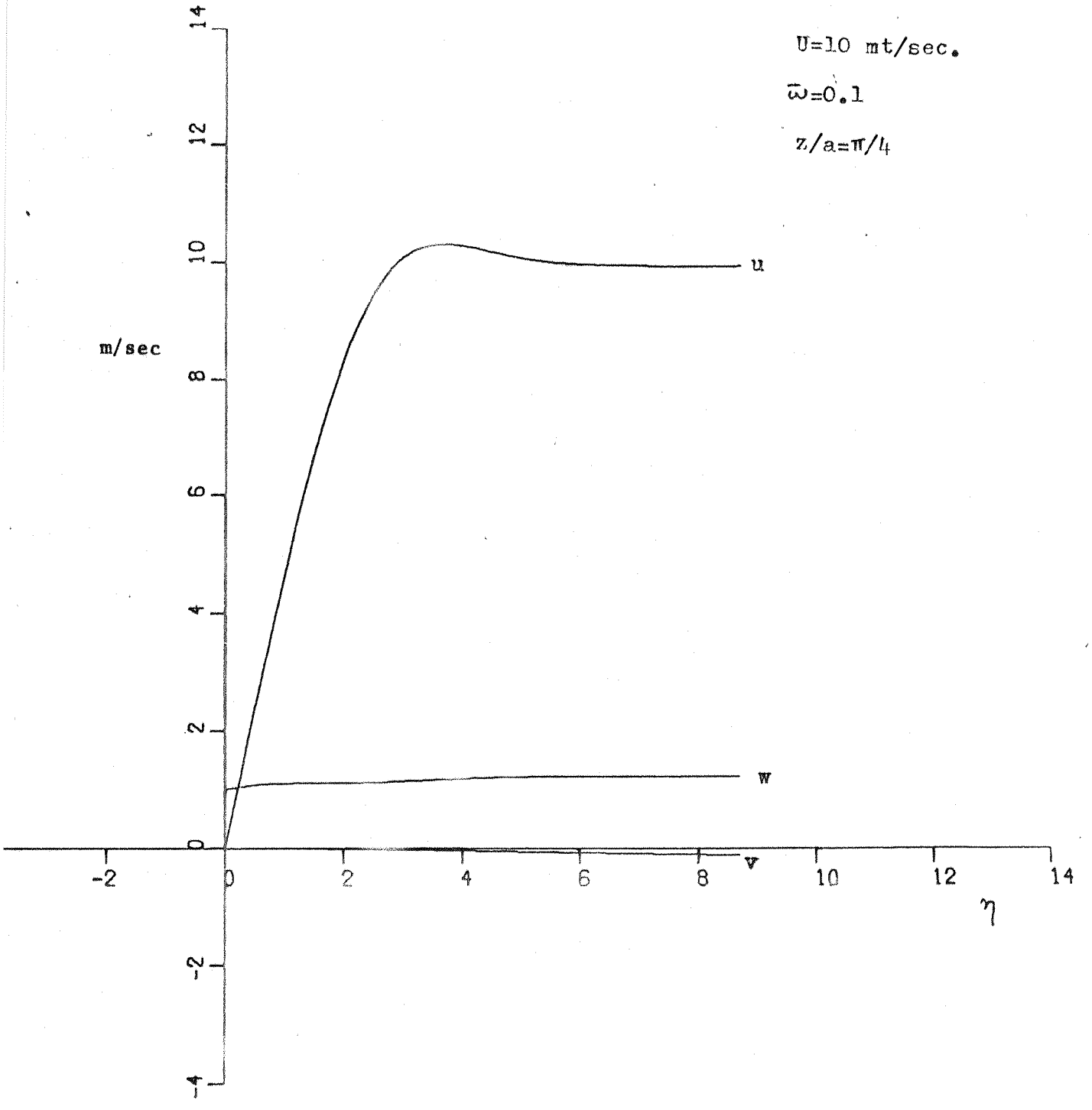

Fig(11.3) velocity profiles of a rotating cylinder

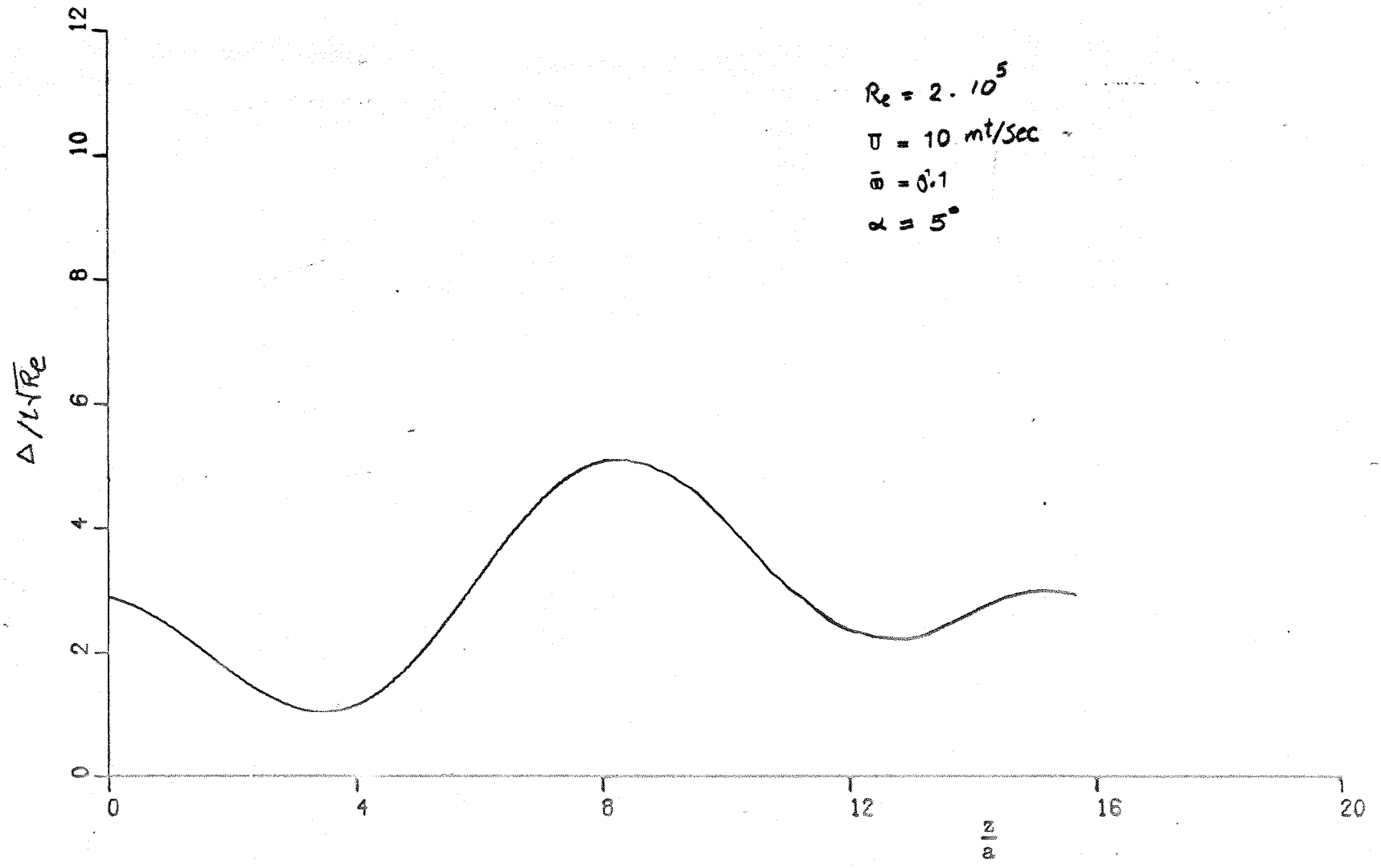

FIG.(II.4) BOUNDARY LAYER THICKNESS DISTRIBUTION

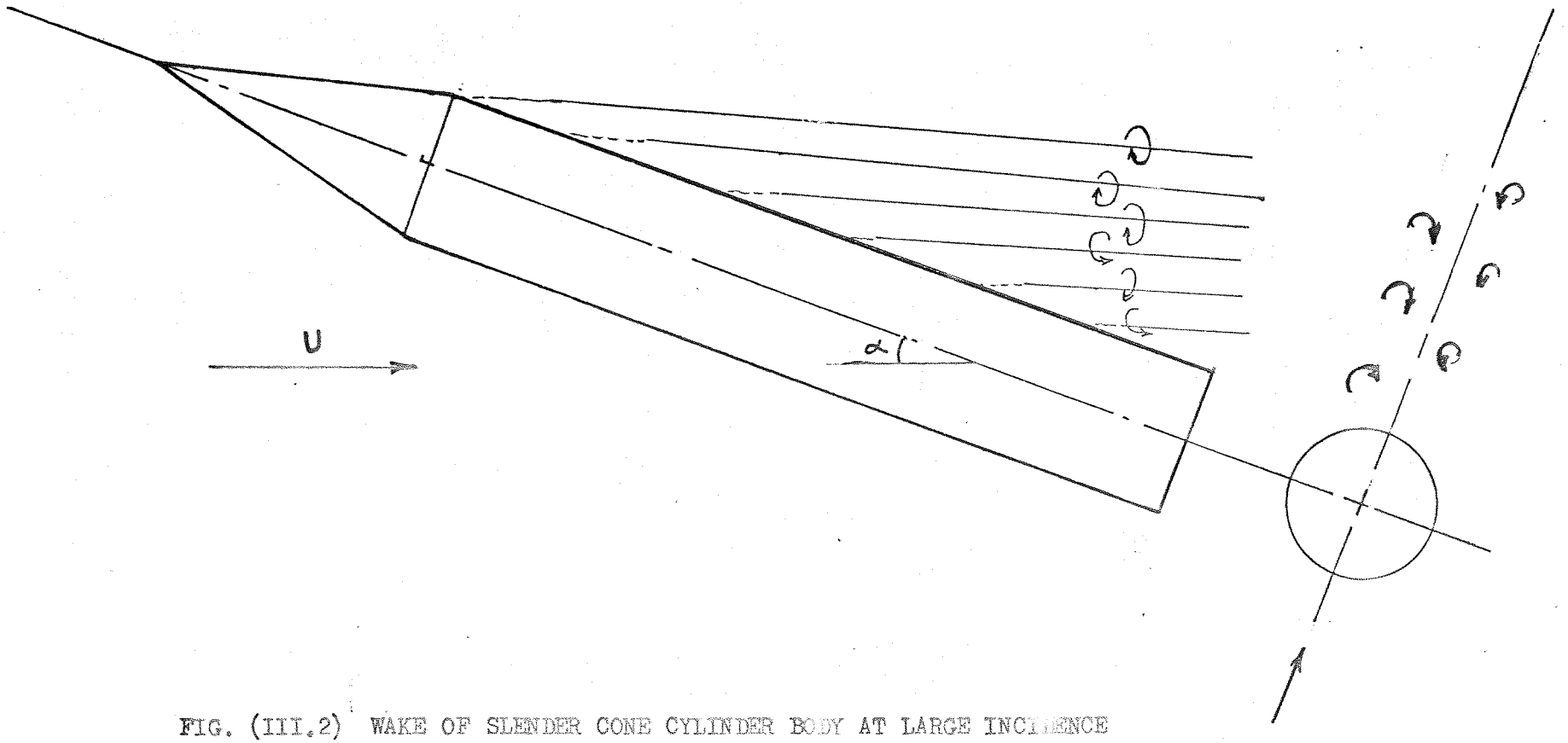

FIG. (III.2) WAKE OF SLENDER CONE CYLINDER BODY AT LARGE INCIDENCE

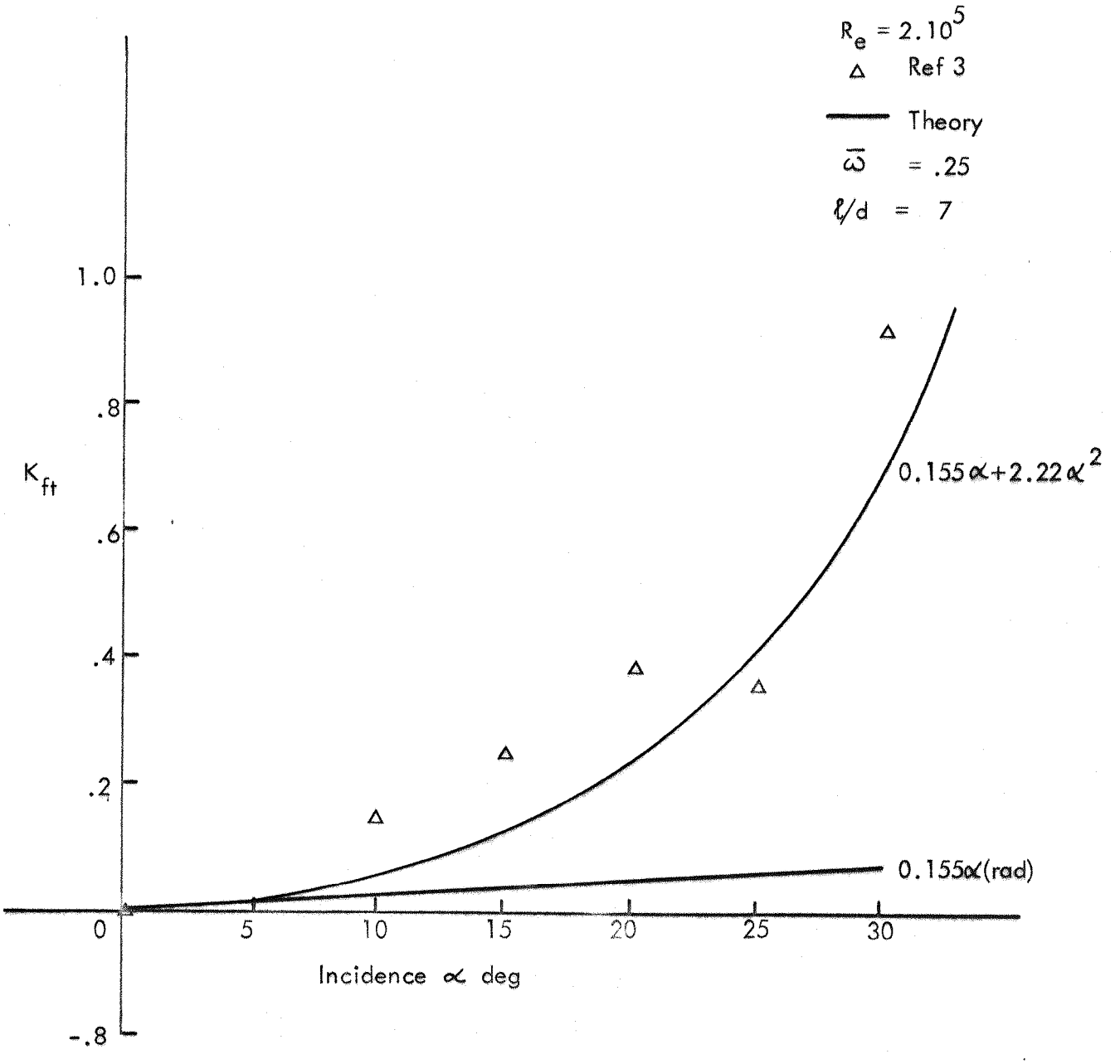

FIG. (IV.1) VARIATION OF MAGNUS FORCE COEFFICIENT WITH INCIDENCE.

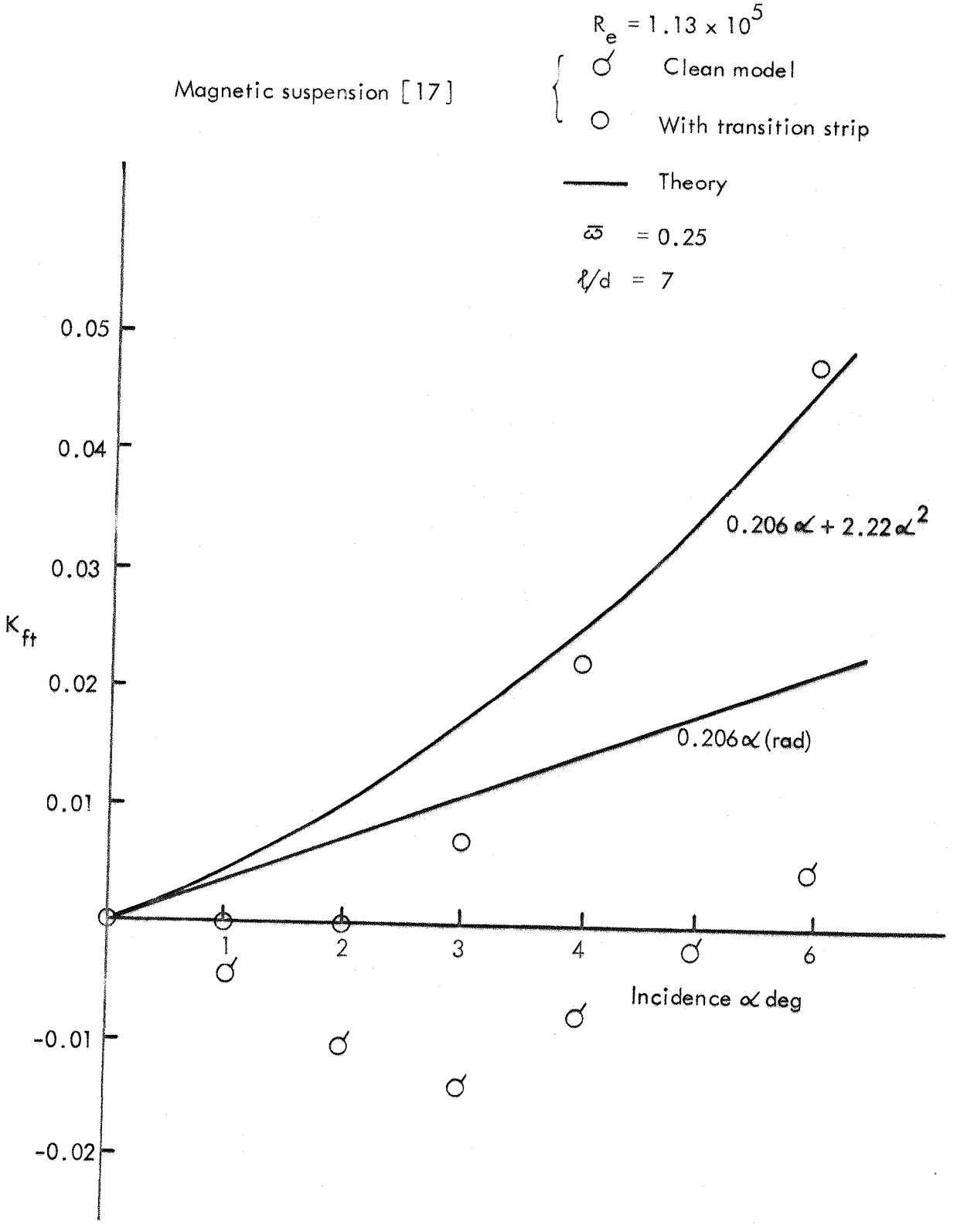

FIG. (IV.2) VARIATION OF MAGNUS FORCE COEFFICIENT WITH INCIDENCE.

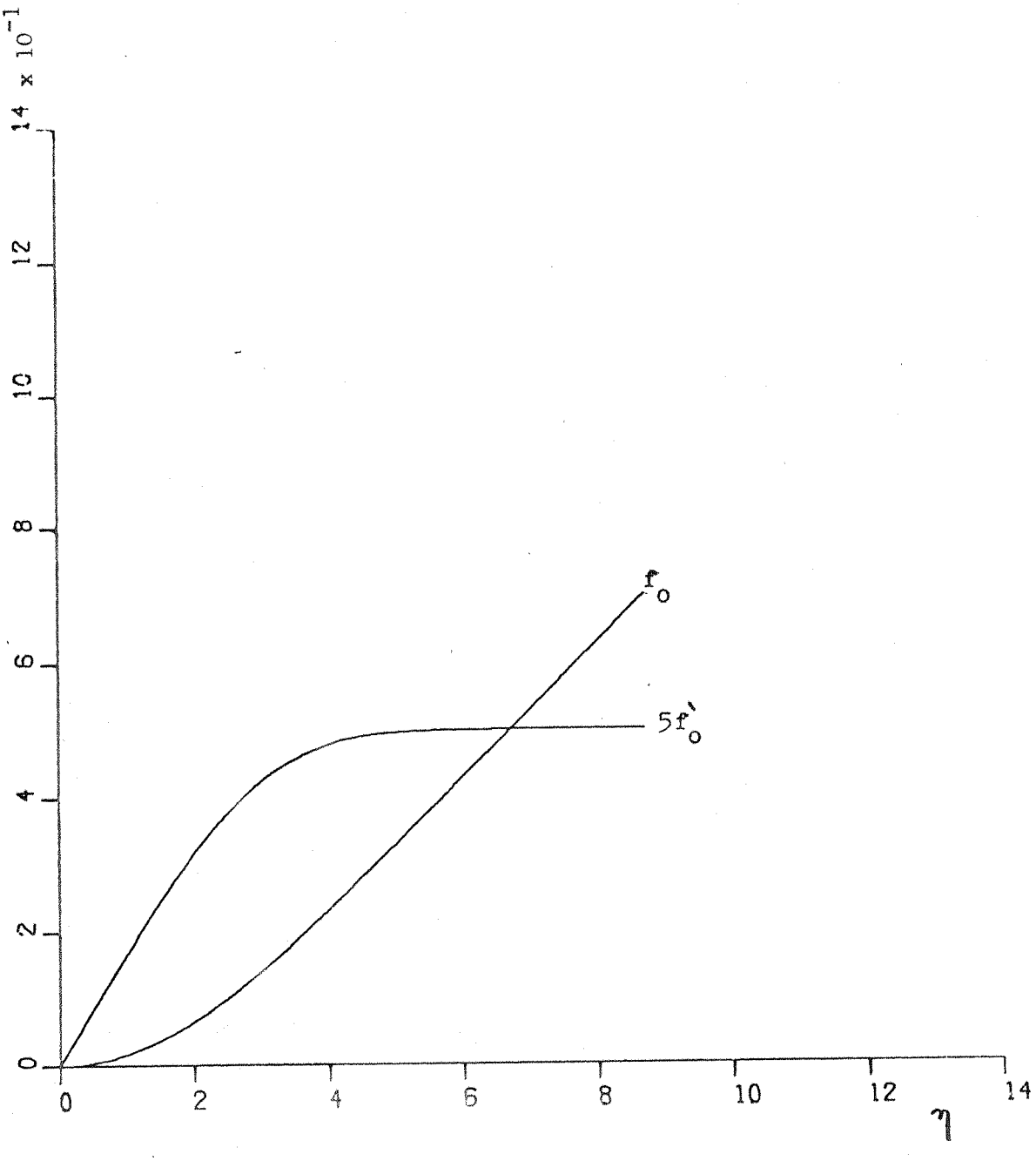

Fig(A.1) variation of perturbation functions f_o, $5f_o'$ with η

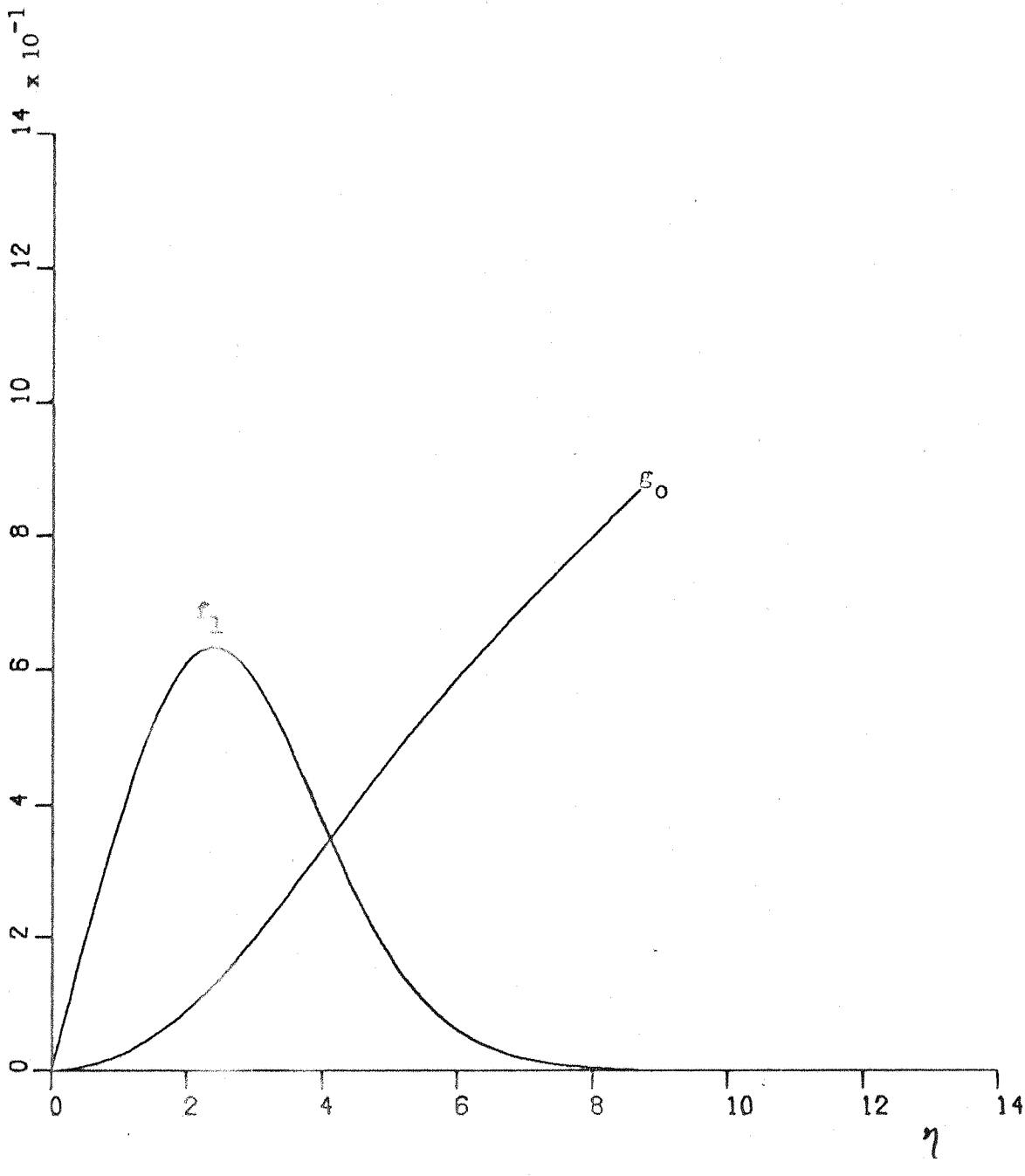

Fig(A.2) variation of perturbation functions f_1, g_o with η

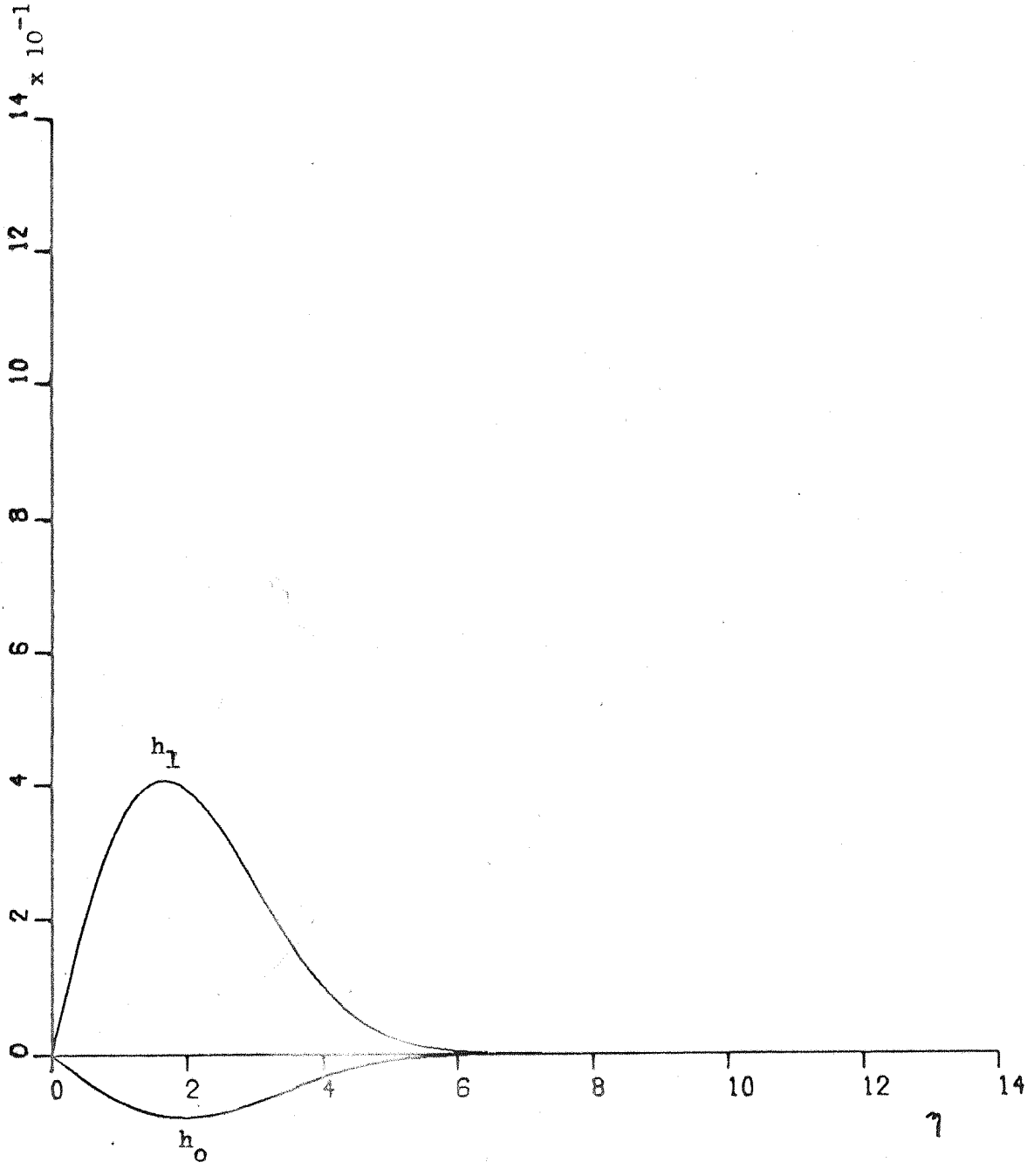

Fig(A.3) variation of perturbation functions h_o, h_1 with η

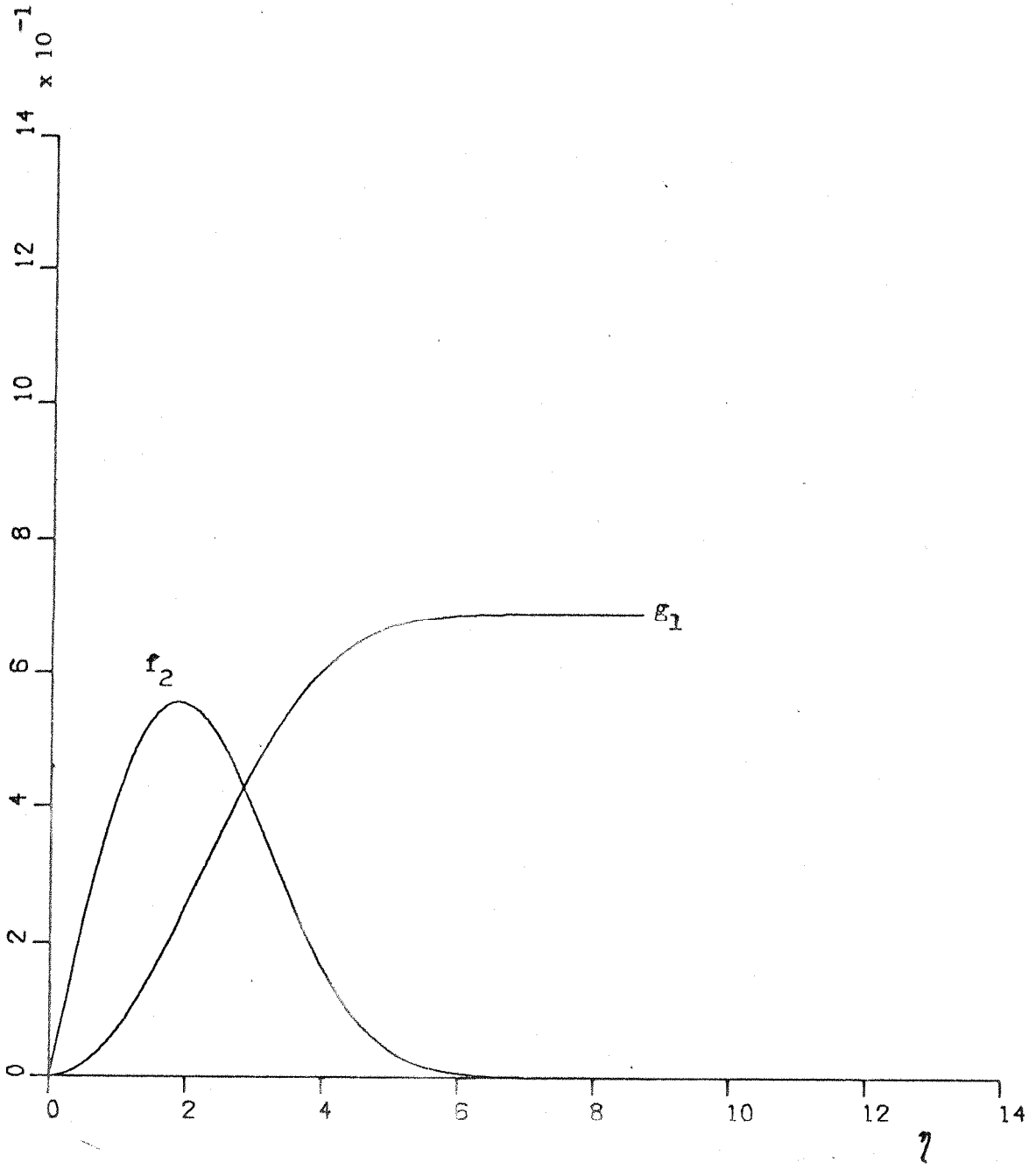

Fig(A.4) variation of perturbation functions f_2, g_1 with η

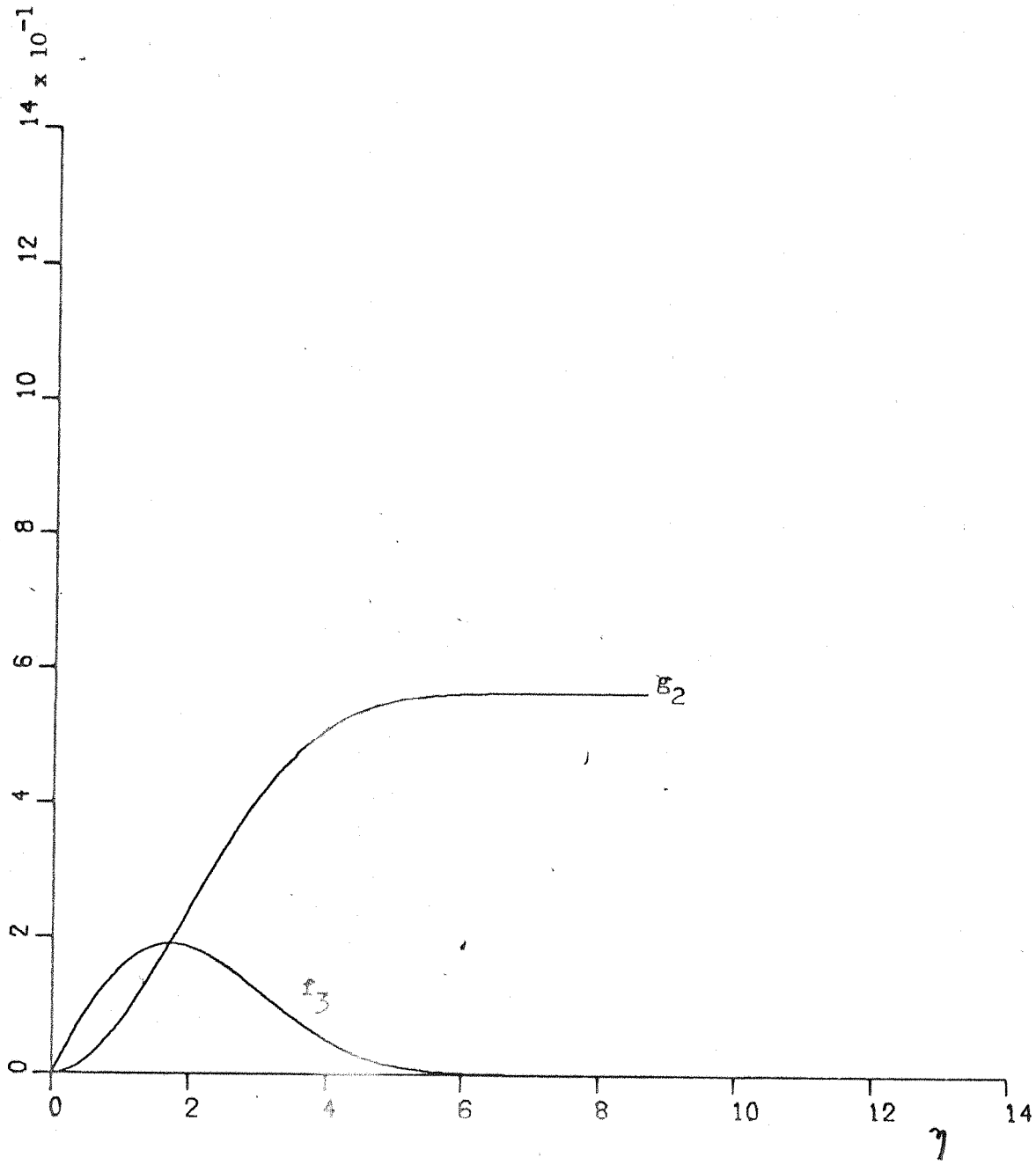

Fig(A.5) variation of perturbation functions f_3, g_2 with η

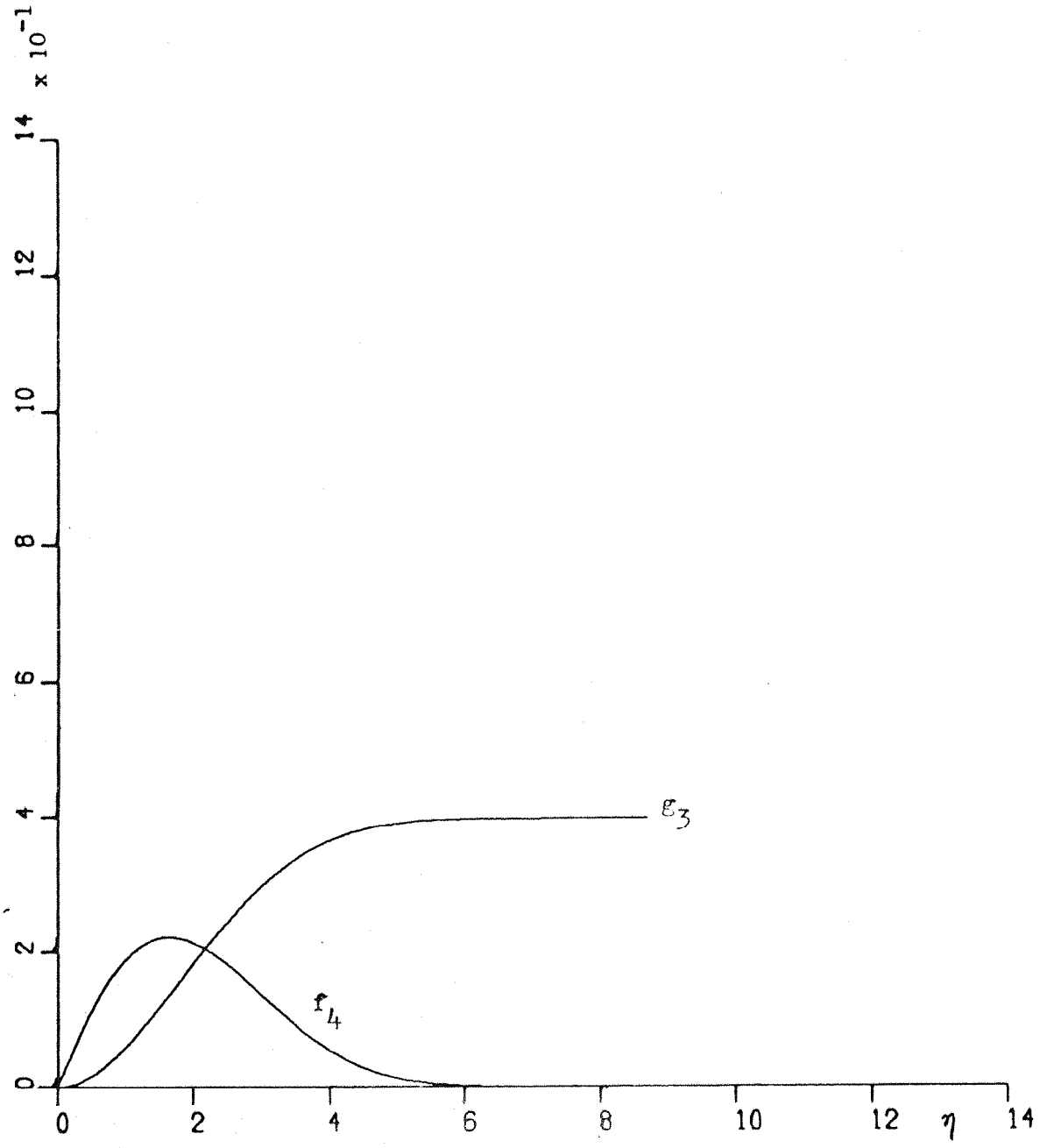

Fig(A.6) variation of perturbation functions f_4, g_3 with η

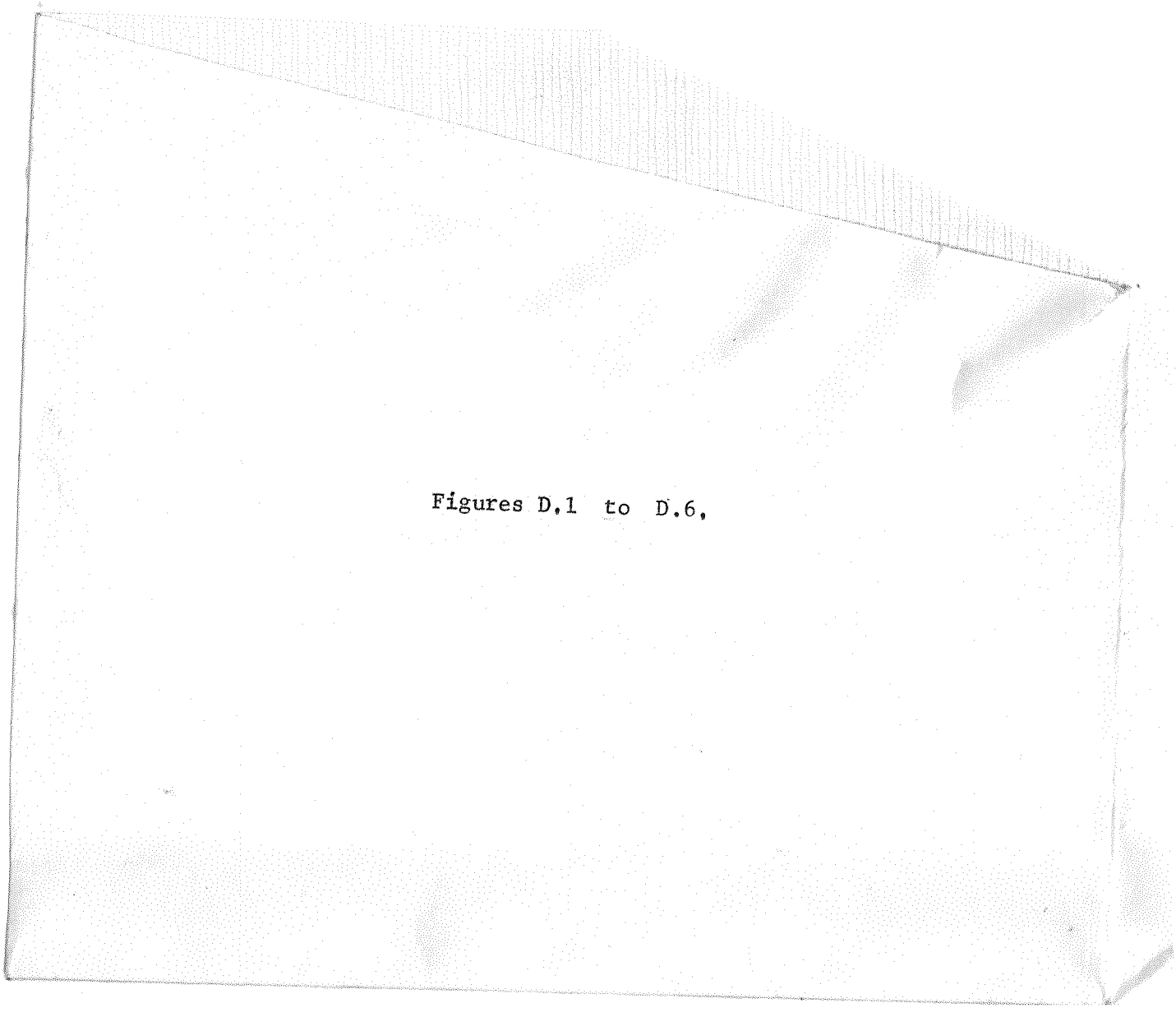

Figures D.1 to D.6.

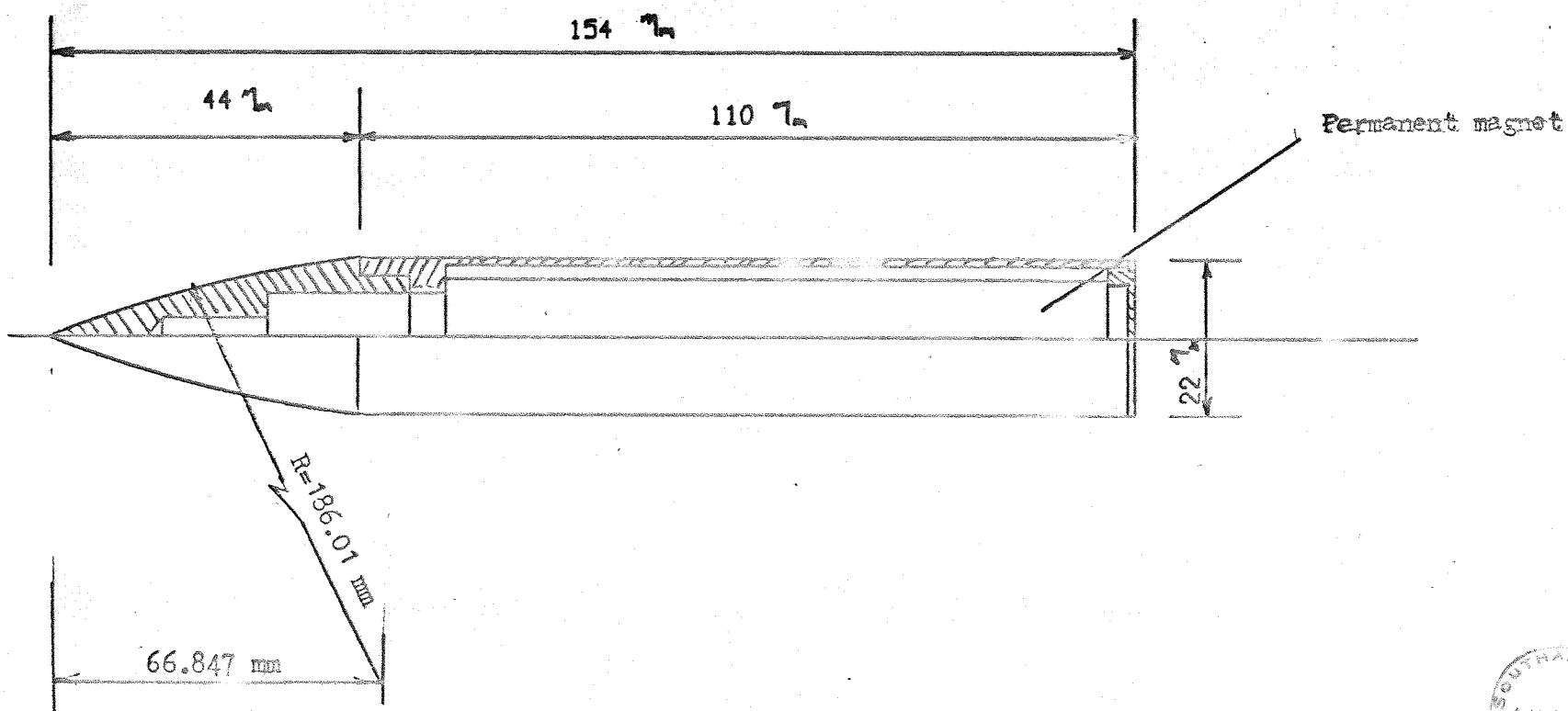

FIG(3.1)MODEL USED IN MAGNETIC SUSPENSION

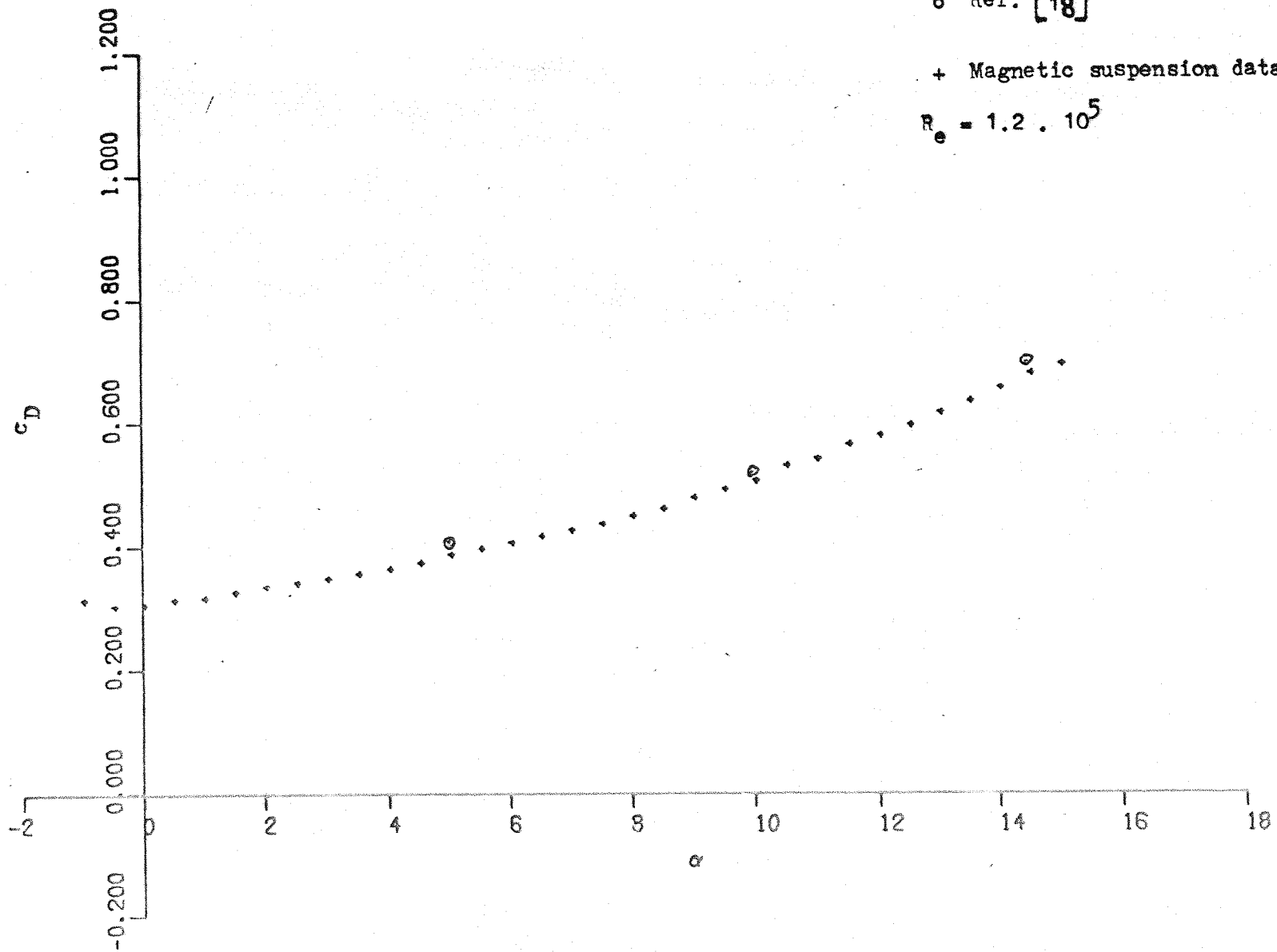

FIG. (D.3) VARIATION OF DRAG COEFFICIENT WITH INCIDENCE

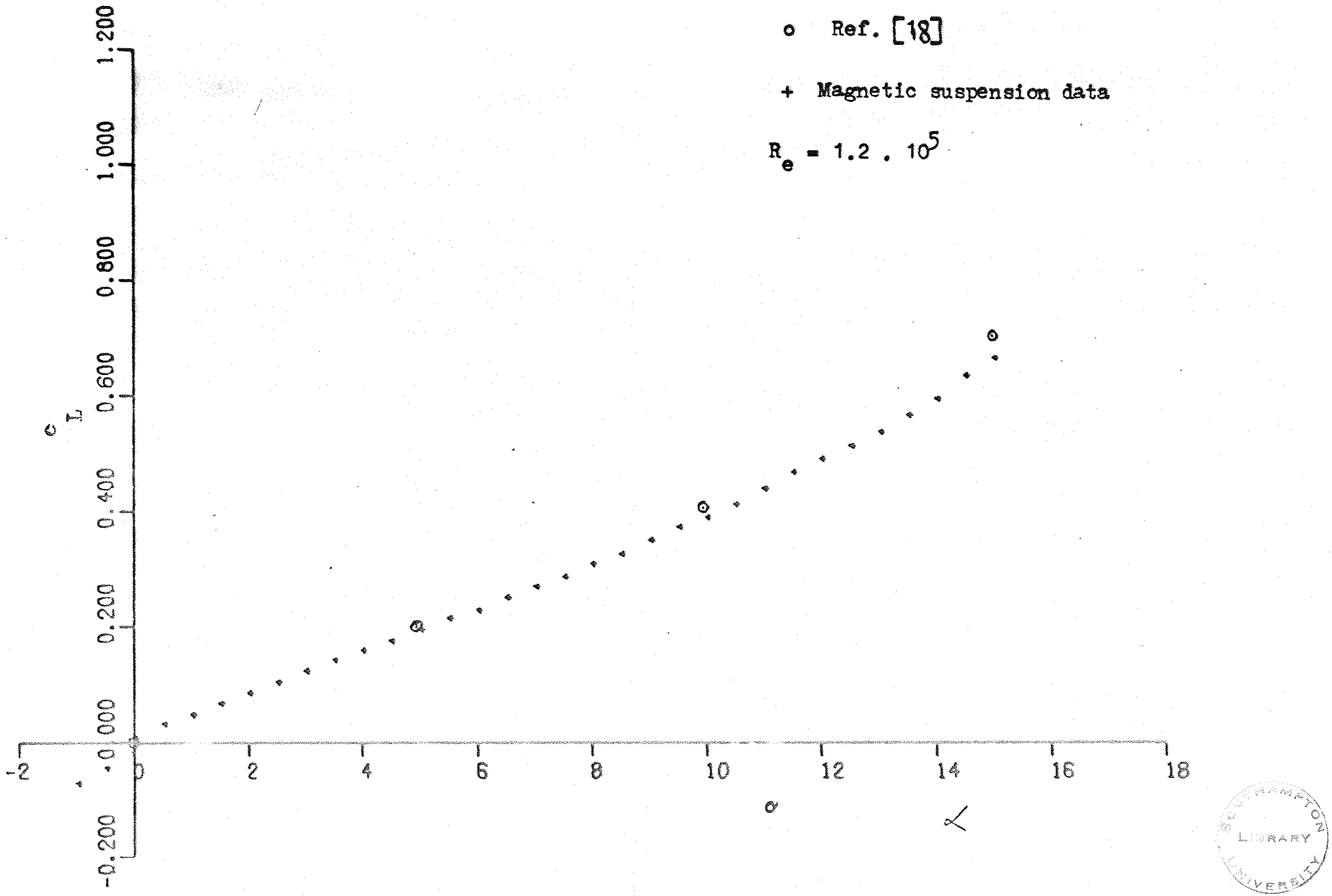

FIG. (D.2) VARIATION OF LIFT COEFFICIENT WITH INCIDENCE

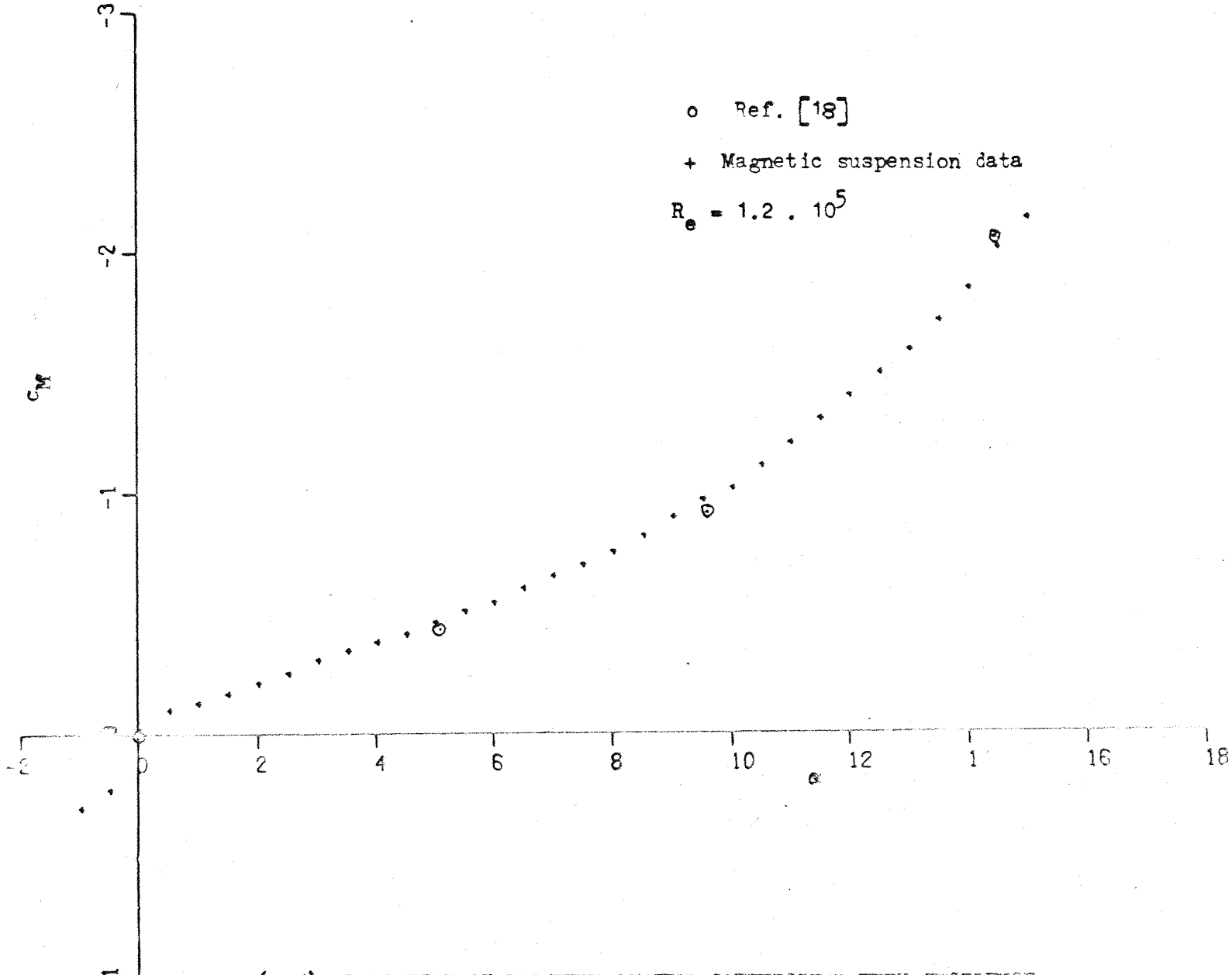

FIG. (D.4) VARIATION OF PITCHING MOMENT COEFFICIENT WITH INCIDENCE

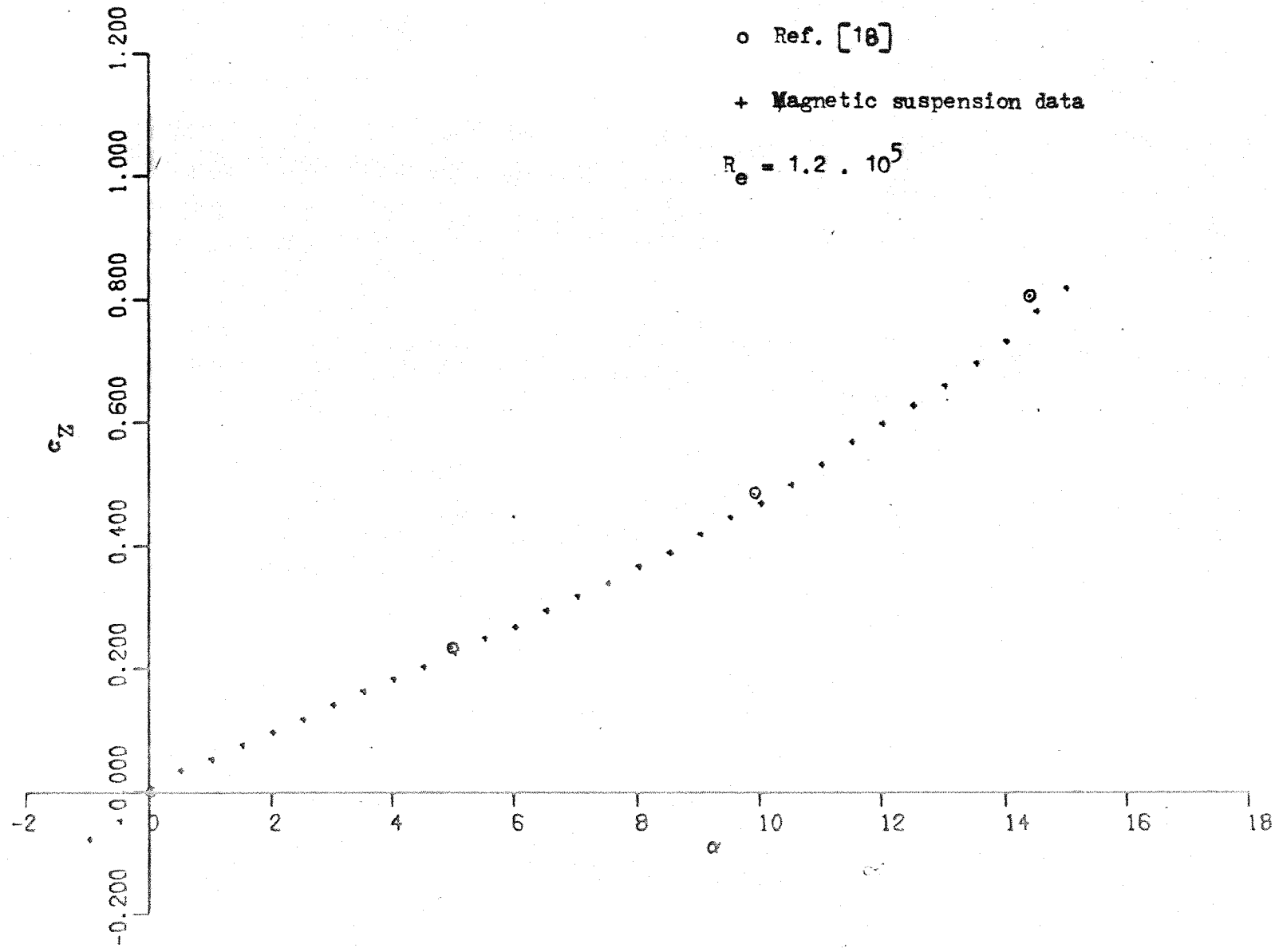

FIG. (D.5) VARIATION OF NORMAL FORCE COEFFICIENT WITH INCIDENCE

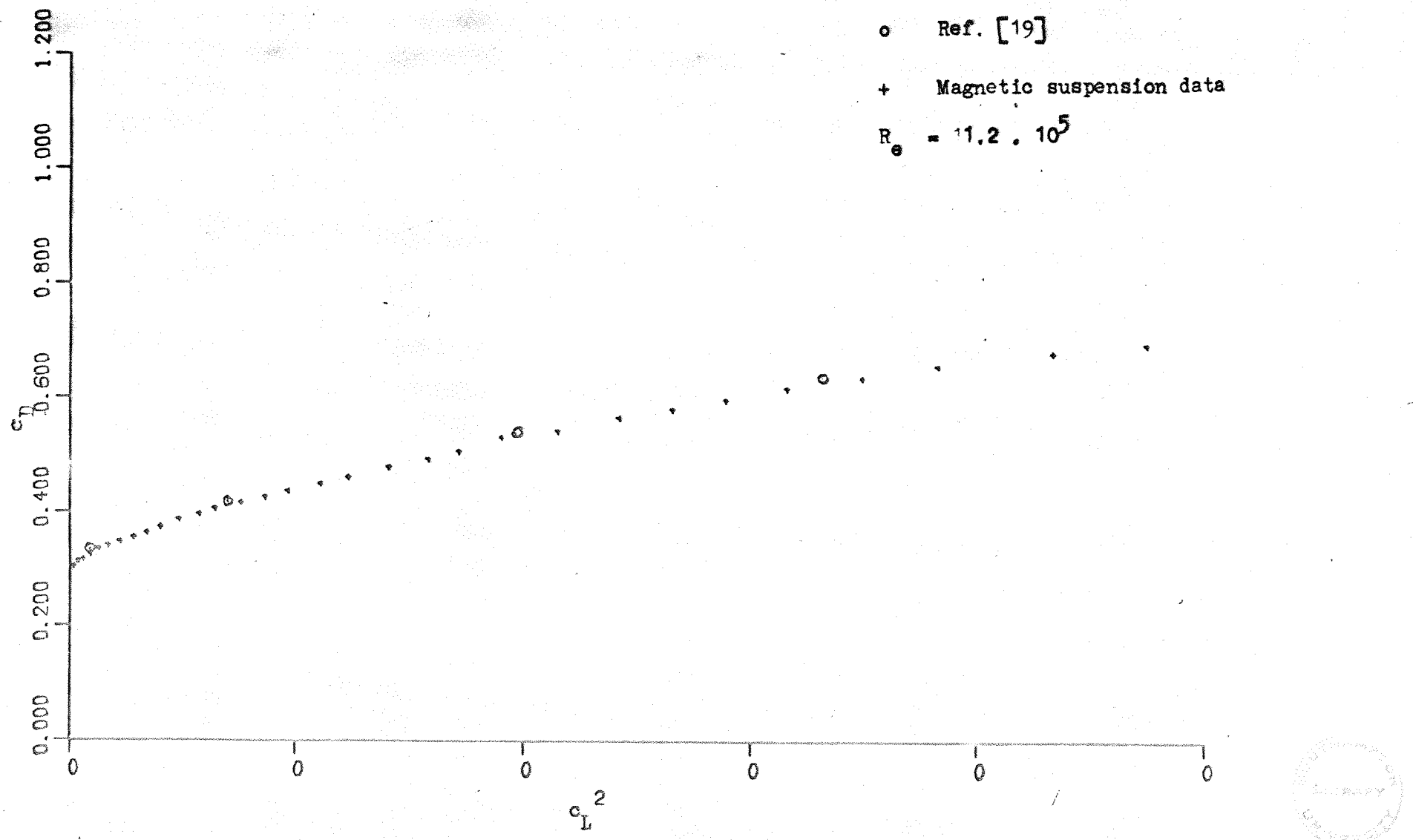

FIG. (D.6) VARIATION OF DRAG COEFFICIENT WITH SQUARE OF LIFT